Potassium Binding Interactions with Aliphatic Amino Acids: Thermodynamic and Entropic Effects Analyzed via a Guided Ion Beam and Computational Study

Roland M. Jones III, Taylor Nilsson, Samantha Walker, and P. B. Armentrout*

Department of Chemistry, University of Utah, 315 S.1400 E. Rm 2020, Salt Lake City, UT 84112,

United States;

ABSTRACT: Noncovalent interactions between alkali metals and amino acids are critical for many biological processes, especially for proper function of protein ion channels; however, many precise binding affinities between alkali metals and amino acids still need to be measured. This study addresses this need by using threshold collision-induced dissociation with a guided ion beam tandem mass spectrometer to measure binding affinities between potassium cations and the aliphatic amino acids: Gly, Ala, hAla, Val, Leu, and Ile. These measurements are supplemented by theoretical calculations and include commentary on effects of enthalpy, entropy, and structural preference. Notably, all levels of theory indicate that the lowest-lying isomers at 298 K have K⁺ binding to the carbonyl oxygen in either a monodentate ([CO]) or bidentate ([CO,OH]) fashion, isomers that are linked in a double-well potential. This complicates the analysis of the data, although does not greatly influence the final results. Analysis of the resulting cross sections includes accounting for multiple ion-molecule collisions, internal energy of reactant ions, and unimolecular decay rates. The resulting experimental bond dissociation energies generally increase as the polarizability of the amino acid increases, results that agree well with quantum chemical calculations done at the B3LYP, B3P86, and MP2(full) levels of theory, with B3LYP-GD3BJ predicting systematically larger values.

INTRODUCTION

Potassium cations serve various essential functions throughout different biological systems. Examples include regulating energetics in the mitochondria, controlling propensity for cell apoptosis, aiding pathogen resistance, and regulating cellular transmembrane potentials. Such processes are enabled by the ability of proteins to distinguish K⁺ from other metal ions, particularly other alkali ions, and to facilitate K⁺ flow across different cell membranes, often against concentration gradients. In these environments, noncovalent interactions are crucial to define metal ion selectivity and effective K⁺ transport where aliphatic amino acids (AAs) govern many of the interactions.

Unfortunately, past experimental methods have struggled to quantify *in vivo* K⁺AA binding affinities because of other interfering interactions in biological systems.¹² A patch clamp method has been used to characterize ion selectivity by measuring the currents of different ions across a channel¹³ while utilizing Erying transition state (TS) theory to extract kinetic information;¹⁴⁻¹⁵ however, the physical determinants of the rate constants used in the theory are still poorly understood, making measurements of a single TS difficult.¹⁶ Nevertheless, the importance of such measurements can be seen in studies showing that just one residue substitution in a channel can change its ion selectivity and function.^{11, 17-21} Such remarkable, yet sensitive, selectivity for K⁺ is complimented by the high throughput rate of these channels that approaches the diffusion limit of K⁺ in solution.²² This high rate is attributed to the center region of potassium channels containing many aliphatic AAs.²³ As such, binding affinity measurements and calculations require great precision to benefit similar studies expanded to larger systems.

One approach to remove interferences from other biological residues and the complexity of the biological system is to measure K⁺ binding affinities individually for each AA or small peptide. These individual measurements can then be combined to help evaluate larger systems. Clearly, limitations associated with the N and C termini remaining need to be recognized, although studies on functionalized AAs that mimic internal residues better offer interesting extensions of the present studies. Rodgers and Armentrout refer to collecting such measurements as building a

"thermodynamic vocabulary" and have measured these pairwise binding affinities between a variety of metal cations and biological residues. 24-42

The metal cation binding affinity of an AA is mainly influenced by the AA conformation and the coordination site of the metal.⁴³ Usually, the AA either takes its canonical form (charge solvated; CS) or the zwitterionic salt-bridge form (ZW).⁴⁴ For instance, Wyttenbach, Witt, and Bowers found that both Na⁺ and Cs⁺ favored a CS complex with glycine (Gly) but a ZW complex with arginine. 45 This suggests that a functionalized side chain can provide stabilizing interactions for the ZW complex, as seen similarly with other functionalized M⁺AAs. ^{32-39, 46} Other studies have collected infrared multiple photon dissociation (IRMPD) spectra of M⁺AAs using analogues of Gly, alanine (Ala), and proline (Pro) with secondary and tertiary amino groups to observe which isomer is more favorable. 47-49 In contrast to functionalized M⁺AAs, the investigators found that stability for the CS form increased with alkali cation size (Li⁺, Na⁺, K⁺, Rb⁺, and Cs⁺) for these systems. Furthermore, IRMPD spectra of aliphatic M⁺AAs with secondary amino groups revealed that Li⁺ and Na⁺ formed exclusively ZW complexes, whereas both the ZW and CS isomers were populated with K⁺, Rb⁺, and Cs⁺.⁴⁷ These findings suggest that increasing alkali metal size increases the stability of the CS form in the absence of functional groups. For such CS systems, the IRMPD study using AA analogues with secondary and tertiary amino groups indicated that the AA favors chelation with the amine and carbonyl oxygen for Li⁺ and Na⁺, whereas K⁺, Rb⁺, and Cs⁺ can also coordinate with just the carboxyl oxygens.⁴⁷ In contrast, the ZW systems showed unambiguous bidentate chelation with the C-terminus oxygens for each metal. Presently, no IRMPD spectra have been published for potassiated aliphatic amino acids, although spectra have been reported for potassiated N-methylalanine, proline, N-methylproline, and N-methylproline methylester.47

Threshold collision-induced dissociation (TCID) and the kinetic method (KM) have been the most common procedures used for characterizing the binding energies of M⁺AA complexes.⁵⁰ Unfortunately, the KM may fail to account for entropic effects that can occur within a system.⁵¹ Current literature values for binding affinities between K⁺ and aliphatic AAs have been measured

by Tsang and coworkers using the KM,⁵² while other studies have obtained values through theoretical calculations.^{24, 52-55} Among the aliphatic AAs, only the K⁺Gly binding affinity has been measured using TCID with a guided ion beam tandem mass spectrometer (GIBMS).²⁴ In order to properly account for entropic effects, the present study aims to utilize a GIBMS to measure dissociation enthalpies of K⁺ complexed with Gly, Ala, α-aminobutyric acid (homoalanine, hAla), valine (Val), leucine (Leu), and isoleucine (Ile) at 0 K. These experimental values are compared with values obtained from theoretical calculations using several levels of theory that previous studies on similar systems in our lab have shown are reliable.^{28, 30, 56-59} Theoretical calculations also include Gibbs energies at 298 K for structural insights under thermal conditions with particular attention being given to analyzing the energies between related isomers.

EXPERIMENTAL AND COMPUTATIONAL DETAILS

General Experimental Procedures. Cross sections were collected for the dissociation of each K⁺AA complex (AA = Gly, Ala, hAla, Val, Leu, and Ile) induced by collisions with Xe using a GIBMS described in previous work. $^{60-62}$ A diagram of the GIBMS (with a different source) can be found in the latter two references. The gas-phase K⁺AA complexes were generated using an electrospray ionization (ESI) source 63 under ambient conditions. A diagram of the source arrangement used can be found in this reference. Our sample solution comprised 50:50 by volume of H₂O:MeOH (Sigma-Aldrich) with $\sim 10^{-4}$ M AA (Sigma-Aldrich) and $\sim 10^{-3}$ M KCl (Sigma-Aldrich). All AAs used were L-enantiomers as found in biological systems. The solution flow rate was set to 0.05 mL/hour, and the ESI needle voltage ranged from $\sim 1800 - 2200$ V. The ions were then guided by a capillary heated to 80 °C into a radio frequency (rf) ion funnel, 64 where they were collimated into a tightly focused beam and injected into an rf hexapole ion guide, radially trapping the ions. Here, the ions experienced multiple thermalizing collisions (>10⁴) with ambient gas ($\sim 10^{-2}$ Torr) that also entered the instrument through the capillary. As a result, the ions had internal energies well characterized by a Maxwell-Boltzmann distribution of rovibrational states at 300 K, as detailed previously in studies containing alkali metals and other AAs. 25 , 29 , 63 , 65 - 71

Ions were then extracted from the hexapole ion guide, focused into a magnetic momentum analyzer where the K⁺AA ions were mass selected, decelerated to well-defined kinetic energies with an exponential retarder, and collimated into a meter-long dual rf octopole. ^{62, 72-73} This octopole passed through a static collision cell containing Xe at a low enough pressure such that single collisions conditions dominated. Collisions resulted in product ions (exclusively K⁺ here) that drifted to the end of the octopole along with residual reactant ions where they were focused into a quadrupole mass filter for mass analysis. Ions were then detected using a Daly detector. ⁷⁴ The absolute zero of the kinetic energy scale and the reactant ion's kinetic energy distribution were measured using a potential retarding technique in the octopole, as described previously. ⁶⁷ Reactant and product ion intensities (taken from total ion counts) were converted into absolute cross sections for analysis, and the ion kinetic energies in laboratory (Lab) frame were converted to relative energies in the center-of-mass (CM) frame using previously described methods. ⁶⁰⁻⁶¹ In this manuscript, all reported energies are in the CM frame.

Data Analysis. The thermochemical data analysis procedure has been well characterized in past studies⁷⁵⁻⁷⁷ with each cross section in the present study being modeled by Eq. 1.

$$\sigma(E) = \frac{n\sigma_0}{E} \sum_{i} g_i \int_{E_0 - E_i}^{E} \left\{ 1 - e^{-k(E^*)\tau} \right\} (E - \varepsilon)^{n-1} d(\varepsilon)$$
 (1)

Here, σ_0 is an energy-independent adjustable scaling parameter, n is an adjustable parameter characterizing the energy deposition efficiency during a collision, 62 E is the relative (CM) kinetic energy of the reactants, E_0 is the threshold energy for the product channel at 0 K, and ε is the energy transferred from translational motion to internal energy of the reactant ion complex resulting from a collision with Xe. The summation in Eq. 1 is over the rovibrational states of reactant ions, i, such that E_i is the excitation energy of each state and g_i refers to the fractional population of such states where $\Sigma g_i = 1$. Furthermore, $E^* = \varepsilon + E_i$ is the internal energy of the energized molecule (EM) after a collision. The term enclosed within curly brackets refers to the total probability of dissociation for the EM, where τ refers to the experimental time for dissociation

(~5 × 10⁻⁴ s according to time-of-flight studies). As a result, Eq. 1 takes into account the lifetime of dissociation for the EM, which can delay the apparent onset of the product cross section. This kinetic shift increases in magnitude as the molecule becomes larger. Accounting for the kinetic shift is appropriate in this study as kinetic shifts ranging from 0.04 to 0.50 eV were observed in a similar study measuring the sodium cation binding affinities with aliphatic AAs. Each rate constant, $k(E^*)$, was determined by using Rice-Ramsperger-Kassel-Marcus theory, as shown in Eq. 2.79-80

$$k(E^*) = \frac{sN^{\dagger}(E^* - E_0)}{h\rho(E^*)}$$
 (2)

In this equation, s refers to the reaction degeneracy (unity here), $N^{\dagger}(E^*-E_0)$ is the sum of rotational and vibrational states of the TS with an energy E^*-E_0 , ρ (E^*) refers to the density of states of the EM at an available energy of E^* , and h is Planck's constant. Quantum chemical calculations were used to determine values for rotational constants and vibrational frequencies of the TSs and EMs. Because the reactions in this study have rate-limiting loose TSs, the TS frequencies were those of the dissociated products with transitional frequencies treated as rotors in the phase space limit (PSL). T5-76 All 2D external rotations were treated adiabatically while taking centrifugal effects into account. A statistical distribution summed across all possible values for a rotational quantum number was used to quantify the rotational energy. The number and density of rotational and vibrational states were determined using the Beyer-Swinehart-Stein-Rabinovitch algorithm.

Before running this data analysis, it was important to consider several phenomena that could interfere with accurate data interpretation. First, experimental cross sections may not reflect the true single-collision conditions needed for our model. We accounted for this by collecting data at multiple pressures of Xe (generally 0.3, 0.15, and ~0.05 mTorr, although for K⁺Val, only the high and low pressures were utilized) and extrapolating the results to a pressure of zero, rigorous single-collision conditions. ⁸⁴ Second, energy broadening from the thermal motion of Xe (Doppler broadening) and the kinetic energy distribution of the K⁺AA reactant were accounted for by convoluting Eq. 1 with these kinetic energy distributions. ^{60, 85} Lastly, it was assumed that the

measured E_0 was for product formation from the lowest energy reactant ion isomer going to the lowest energy conformer of the products. This assumption is made because the EM should have enough time to rearrange to the ground conformers of the products after collisional excitation. A nonlinear least-squares procedure was then used to optimize the various adjustable parameters in Eq. 1 for comparison to the experimental cross sections. Uncertainties in these parameters were determined by their distributions across different data sets in addition to varying the optimized n value up and down by 10%, scaling vibrational frequencies of reactants, EMs, and TSs up and down by 10%, scaling τ up and down by a factor of 2, and by taking into account the 0.02 eV (CM) uncertainty in the energy scale.

Computational Details. Conformational space was probed using a simulated annealing procedure utilizing the AMBER1486 force field. This procedure has been described in more detail in a previous study²⁹ and was implemented here to find all relevant low-lying structures of the potassiated amino acids. Briefly, the AMBER suite of programs and AMBER force field were used to generate starting structures. All unique structures from this were then optimized using NWChem6.8 at the HF/3-21G level of theory. From these structures, a final set of structures were minimized using a Berny optimization⁸⁷ at the B3LYP/6-311+G(d,p)⁸⁸⁻⁸⁹ level of theory. This basis set was chosen because previous studies by Moision and Armentrout²⁴ and Wong et al.⁵⁵ concluded that it was sufficient to find the low-energy isomers and conformers, whereas some isomers were not stable when using smaller basis sets. Single-point energies (SPEs) were calculated at the B3LYP, B3P86, and MP2(full) (where full refers to the correlation of all electrons, abbreviated as MP2 below) levels of theory using the 6-311+G(2d,2p) basis set and the B3LYP/6-311+G(d,p) geometries. Zero-point energy (ZPE) corrections and thermal corrections at 298 K were determined using vibrational frequencies scaled by 0.989.90 This procedure was also repeated using the D3 Grimme dispersion⁹¹ with Beck-Johnson damping⁹² (GD3BJ) by minimizing the final set of structures using B3LYP-GD3BJ/6-311+G(d,p) and calculating SPEs at B3LYP-GD3BJ/6-311+G(2d,2p). Previous studies have shown that these levels of theory and basis sets provide accurate comparisons with bond dissociation energies (BDEs) between sodium or potassium cations and AAs. ^{12, 25, 29, 41-42, 46, 78, 93} The BDEs were then equated to the difference between the total energy of the K⁺AA complex and the sum of the energies of the individual K⁺ and AA as shown in Eq. 3.

$$D_0(K^+ - AA) = E_{AA} + E_{K^+} - E_{Complex}$$
 (3)

Basis set superposition errors (BSSE) in the BDEs were also estimated using the full counterpoise method.⁹⁴

Nomenclature. The nomenclature used in this study for naming low-energy isomers and conformers of AA and K⁺AA complexes matches that used in previous work.^{27,78} Specifically, the AA is labeled with its three letter code followed by the metal coordination sites within brackets. As such, CO refers to the carbonyl oxygen, N refers to the amine nitrogen, OH refers to the hydroxyl group, and CO2- refers to both oxygen atoms of the carboxylate group binding in a bidentate fashion formed when the OH proton has migrated to the amine nitrogen atom (zwitterion). Atoms simultaneously coordinating with K⁺ are separated by a comma to indicate bidentate coordination (except for the CO₂⁻ group, which is intrinsically bidentate). The two dihedral angles of each AA backbone are labeled beginning from the proton on the OH group (or hydrogen bonded to the oxygen in zwitterionic structures) and terminating with the nitrogen, i.e., ∠HOCC and ∠OCCN. This is followed by the dihedral angles for the side chain in parentheses beginning with the carbon on the carboxylic acid and terminating with the last carbon on the side chain (hAla and IIe) or the hydrogen connected to the β (for Val) or γ carbon (for Leu). These dihedral angles are identified as c (cis for angles below 50°), g (gauche for angles between 50° and 135°), and t (trans for angles above 135°). If two different conformers have the same chelation site and dihedral angle configurations, then wherever an angle differs in sign (positive or negative), a + or – subscript is added. Also, for such cases, an S (syn) is added if the K⁺ is located on the same side of the AA backbone as the side chain, and an A (anti) is added if it is located on the opposite side.

RESULTS

Cross Sections for Collision-Induced Dissociation. Experimental cross sections were collected for collision of Xe with K⁺Gly, K⁺Ala, K⁺hAla, K⁺Val, K⁺Leu, and K⁺Ile, Figure 1. The only process observed at the energies and pressures used was the loss of the intact neutral ligand through the collision-induced dissociation (CID) reaction 4.

$$K^{+}AA + Xe \rightarrow K^{+} + AA + Xe \tag{4}$$

Zero-pressure extrapolated cross sections for each system are shown Figure 1. In all cases, cross sections increase quickly from energies near 1 eV and begin to level around 3 to 4 eV with magnitudes of $(10 - 30) \times 10^{-16}$ cm². Fluctuations in cross sections observed near 4 eV (e.g., for K⁺hAla) are results of focusing aberrations in the reactant ion beam.

Theoretical Results: Global Minima Structures and Low-Energy Isomers of Potassiated Amino Acids. Our calculations indicate that the global minimum (GM) of every K+AA structure adopts either a [CO] or [CO,OH] conformation at 298 K. At 0 K, the same result occurs except the B3LYP-GD3BJ level of theory predicts an [N,CO] GM for the K+Ala, K+Val, K+Leu, and K+Ile systems. Other higher-energy chelation sites include [CO₂-], [N,OH], [N], and [OH]. All these possible coordination motifs are shown in Figure 2 for the example of K+Ala. Structures for the K+AA complexes of other the aliphatic AAs can be found in the Supplementary Materials along with a complete listing of the remaining structures located and their energies, Tables S1 – S4. Tables provided here list only the lowest energy isomers of each type of coordination at 0 and 298 K. For the unmetalated AAs, a list of conformers and their relative energies calculated at the same levels of theory used here can be found in previous work. ⁷⁸ In all cases, the GM neutral AA ligands located theoretically agree with spectroscopic determinations of their conformations in previous studies. ⁹⁵⁻¹⁰⁴

K⁺**Glycine.** Our calculations identify the 0 K GM of the K⁺Gly complex as Gly[CO]cc at the B3LYP and B3P86 levels of theory and Gly[CO,OH]cc at the MP2 and B3LYP-6D3BJ levels of theory, with energies listed in Table 1. At 298 K, the GM remains the same for the B3LYP, B3P86, and MP2 levels of theory but switches to Gly[CO]cc for B3LYP-GD3BJ, Table 1. These

findings are in agreement with previous work by Moision and Armentrout that identified Gly[CO,OH]cc as the 0 K GM at the MP2/6-311+G(2d,2p) level of theory. Lau et al.⁵⁴ (B3LYP/6-311+G(3df,2p)) and Tsang et al. (B3LYP/6-31G(d)) also found a Gly[CO,OH]cc GM at 0 K;⁵² however, in neither of these two studies did the authors list any Gly[CO] isomers. Another study by Wong et al.⁵⁵ identified Gly[CO,OH]cc as the 0 K GM at the B3LYP/6-311+G(3df,2p) level while also listing the Gly[CO]tc isomer, which lies 33.2 – 33.5 kJ mol⁻¹ above their GM depending on their method of geometry optimization. Here, we find this species lies 35 – 39 kJ mol⁻¹ above the GM, Table S1. Our calculations further indicate that at both temperatures the next lowest energy isomers for each chelation site are Gly[N,CO]tt, Gly[CO₂⁻]cc, Gly[N,OH]tc, Gly[N]tt, and Gly[OH]tt, respectively, at all four levels of theory. Our calculations also indicate that it is more energetically favorable for K⁺ to bind with the carbonyl oxygen, as Gly[N,OH]tc, Gly[N]tt, and Gly[OH]tt are all at least 36 kJ mol⁻¹ higher in energy than the GM.

In order to determine what isomers might be formed as reactants at room temperature, we calculated Maxwellian equilibrium distributions at 298 K among Gly[CO]cc, Gly[CO,OH]cc, Gly[N,CO]tt, and Gly[CO₂⁻]cc. These results indicate that these species should comprise 57, 39, 4, and 0.1% at the B3LYP level; 56, 43, 1, and 0.2% at the B3P86 level; and 51, 36, 13, and 0.1% at the B3LYP-GD3BJ level of theory, respectively. These predictions are fairly similar, whereas the 27, 65, 8, and 0.4% predictions at the MP2 level differ somewhat.

K⁺**Alanine.** Ala[CO,OH]cc was found as the 0 K GM for K⁺Ala, Table 1, for all levels of theory used here. This result agrees with work by Marino et al.⁵³ using B3LYP/6-311++G(d,p), Lau et al.⁵⁴ using B3LYP/6-311+G(3df,2p), Tsang et al. using B3LYP/6-31G(d), and Talley et al.¹⁰⁶ (at 298 K) using MP2/LACVP;⁵² however, no Ala[CO] isomer was listed in these studies. In contrast, we find the Ala[CO]cc isomer to be the GM at 298 K according to the B3LYP, B3P86, and B3LYP-GD3BJ levels of theory. Ala[CO,OH]cc remains the GM at this temperature at the MP2 level of theory and is the second lowest energy isomer at the other levels of theory. At both temperatures, our calculations further identify Ala[N,CO]tts followed by Ala[CO₂-]cc as the next

lowest energy chelation sites at every level of theory except for the B3P86 level of theory where Ala[CO₂⁻]cc is lower in energy, Table 1.

Note that in addition to the Ala[N,CO]tts conformer, there is also Ala[N,CO]ttA, Figure 2, which lies 1.5 - 3.2 kJ mol⁻¹ higher in energy. Although the potassium ion chelates to the amino nitrogen and carbonyl oxygen in both cases, the ion is tilted towards the side-chain (syn) in the tts conformer and tilted away (anti) in the ttA conformer. The long-range interaction of the ion with the side-chain helps stabilize this complex, as also noted previously for the analogous sodiated species. ⁷⁸ According to the B3LYP and B3P86 levels of theory, Ala[N,OH]tc_A is the next lowest energy isomer, whereas the MP2 and B3LYP-GD3BJ levels indicate that Ala[N,OH]tcs is slightly lower in energy. Every level of theory agrees that the next lowest energy chelation sites are Ala[N]tt and Ala[OH]tt at both temperatures. the methyl side chain can help stabilize K⁺ coordination via charge-induced dipole interactions. For instance, this effect is apparent in the Ala[N]tt isomer where K⁺ is shifted slightly toward the side chain. Regarding reactant populations, Maxwellian equilibrium distributions at 298 K among Ala[CO]cc, Ala[CO,OH]cc, Ala[N,CO]tts, and Ala[CO₂⁻]cc indicate that these species should comprise 55, 40, 3, and 2% at the B3LYP level; 53, 43, 1, and 2% at the B3P86; and 50, 38, 10, and 2% at the B3LYP-GD3BJ level of theory, respectively. Again the prediction of the MP2 level, 23, 63, 12, and 3%, respectively, differs somewhat.

K⁺**Homoalanine**. We have no knowledge of any prior studies identifying K⁺hAla structures. For each coordination type, there are potentially three side chain orientations (\angle CC^αC^βC^γ is t, g₊, and g₋, with t being favored for isolated hAla). All these possibilities are included in Table S1, with Table 2 including only those that are lowest in energy for each type at some level of theory. At 0 K, our calculations identify the GM as hAla[CO,OH]cc(t) according to the B3LYP, B3P86, and MP2 levels of theory, whereas the B3LYP-GD3BJ level of theory identifies hAla[N,CO]tts(g₋) as the GM, Table 2. These structures are shown in Figure 3. At 298 K, hAla[CO]cc(t) is identified as the GM as it is more favored entropically than hAla[CO,OH]cc(t) by the B3LYP, B3P86, and B3LYP-GD3BJ levels of theory, whereas the MP2 level of theory

retains hAla[CO,OH]cc(t) as the GM. Theory indicates that there are three favorable $hAla[N,CO]tt_S(t)$ is more favorable according to the B3LYP and MP2 levels of theory, whereas $hAla[N,CO]tt_S(g_-)$ is more favorable according to the B3P86 and B3LYP-GD3BJ levels of theory, Table 2. Examination of the structures reveals that $hAla[N,CO]tt_S(g_-)$ has its ethyl side chain rotated closer to K^+ , which the B3P86 and B3LYP-GD3BJ levels of theory indicate favorably ligates with K^+ . Similar interactions between the cation and alkyl groups were also observed by Rodgers and Armentrout for alcohols complexed with lithium¹⁰⁷ and sodium.¹⁰⁸ Theory also indicates that $hAla[CO_2^-]cc(t)$ is similar in energy to both of the hAla[N,CO] conformers with the side chain rotated away from K^+ . As seen with glycine and alanine, the energies of any additional isomers become significantly higher with $hAla[N,OH]tc_A(t)$ followed by hAla[N]tc(t) and $hAla[N]tc(g_-)$, respectively. The only level of theory that predicts $hAla[N]tc(g_-)$ is lower in energy than hAla[N]tc(t) is MP2 at 298 K. Structurally, hAla[N]tc(t) has its side chain rotated towards K^+ , allowing a favorable electrostatic interaction between the side chain and K^+ .

Regarding reactant populations, Maxwellian equilibrium distributions at 298 K among hAla[CO]cc(t), hAla[CO,OH]cc(t), hAla[N,CO]tts(g_-), hAla[N,CO]tts(t), and hAla[CO₂-]cc(t) indicate that these species should comprise 52, 41, 1, 3, and 4% at the B3LYP level; 50, 43, 1, 1, and 5% at the B3P86 level; and 36, 31, 16, 14, and 4% at the B3LYP-GD3BJ level of theory, respectively. Again the MP2 level prefers the [CO,OH] structure more strongly with predicted populations of 20, 64, 0.02, 11, and 5%, respectively.

K⁺**Valine.** For K⁺Val complexes, there are again three potential side chain orientations (\angle CC^αC^βH is t, g₊, and g₋) for each metal coordination type. Our calculations indicate that that Val[CO,OH]cc(g₊) is the 0 K GM by the B3LYP, B3P86, and MP2 levels of theory, Figure 3, whereas Val[N,CO]tt_S(g₊) is the GM by the B3LYP-GD3BJ level of theory. Our B3LYP results are consistent with B3LYP/6-311+G(3df,2p) results from Lau et al.⁵⁴ and B3LYP/6-31G(d) results of Tsang et al.⁵² Neither study lists a Val[CO] isomer, whereas our calculations indicate that Val[CO]cc(g₊) is the GM at 298 K at the B3LYP and B3LYP-GD3BJ levels of theory.

Val[CO,OH]cc(g₊) remains the GM at 298 K for B3P86 and MP2, Table 2.

The different levels of theory used here disagree as to what is the next lowest energy isomer. At both temperatures, $Val[CO_2^-]cc(g_+)$ is listed as the next lowest energy isomer by the B3LYP and B3P86 levels of theory, whereas $Val[N,CO]tt_S(g_+)$ is identified to have a lower energy by the MP2 and B3LYP-GD3BJ levels of theory, Table 2. $Val[N,CO]tt_A(g_+)$ was also identified as a low-energy isomer with B3LYP and B3P86 predicting it is nearly isoenergetic with the $tt_S(g_+)$ analogue, whereas MP2 and B3LYP-GD3BJ put it 2.3 - 3.7 kJ mol⁻¹ higher. Similar to the systems above, $Val[N,OH]tc_A(g_+)$ and $Val[N]tt(g_+)$ were identified but have much larger energies, Table 2.

Maxwellian equilibrium distributions at 298 K among Val[CO]cc(g₊), Val[CO,OH]cc(g₊), Val[N,CO]tt_S(g₊), and Val[CO₂⁻]cc(g₊) indicate that these species should comprise 45, 44, 2, and 9% at the B3LYP level; 43, 46, 1, and 11% at the B3P86 level; and 33, 33, 23, and 10% at theB3LYP-GD3BJ level of theory, respectively. Again the prediction of the MP2 level, 16, 61, 12, and 11%, respectively, populates the [CO,OH] species more strongly.

K*Leucine. The K*Leu complexes potentially have nine distinct side chain orientations (three each for two dihedral angles) for each metal coordination type. At 0 K, our calculations identify Leu[CO,OH]cc(tg+) as the GM by the B3LYP, B3P86, and MP2 levels of theory, Figure 3, whereas B3LYP-GD3BJ identifies Leu[N,CO]tts(tg+) as the GM, Table 3. The B3LYP, B3P86, and MP2 results are in agreement with Lau et al. who reported Leu[CO,OH] as the GM at the B3LYP/6-311+G(3df,2p) level of theory. Again, neither study mentions a [CO] isomer. At 298 K, Leu[CO]cc(tg+) is identified as the GM and is more entropically favored than Leu[CO,OH]cc(tg+) by the B3LYP, B3P86, and B3LYP-GD3BJ levels of theory, whereas the MP2 level of theory identifies Leu[CO,OH]cc(tg+) as the 298 K GM. Similar to K*Val, theory disagrees as to what is the next lowest energy isomer. At both temperatures, Leu[CO2¯]cc(tg+) is lower in energy than Leu[N,CO]tts(tg+) at the B3LYP and B3P86 levels of theory, whereas MP2 and B3LYP-GD3BJ indicate that Leu[N,CO]tts(tg+) is lower in energy. All four levels of theory agree that at both

temperatures $\text{Leu}[N,OH]\text{tc}_S(tg_+)$ is the next lowest energy chelation site followed by $\text{Leu}[N]\text{tt}(g_-c)$.

Maxwellian equilibrium distributions at 298 K among Leu[CO]cc(tg₊), Leu[CO,OH]cc(tg₊), Leu[N,CO]tt_S(tg₊), and Leu[CO₂⁻]cc(tg₊) indicate that these species should comprise 49, 43, 3, and 6% (B3LYP); 46, 46, 1, and 7% (B3P86); and 39, 38, 16, and 6% (B3LYP-GD3BJ), respectively. Again the prediction of the MP2 level, 17, 62, 13, and 7%, respectively, differs somewhat.

K*Isoleucine. K*Ile complexes can also have nine distinct side chain orientations for each metal coordination type. At 0 K, Ile[CO,OH]cc(g-t) is identified as the GM by the B3LYP, B3P86, and MP2 levels of theory, Figure 3, whereas the B3LYP-GD3BJ level of theory identifies Ile[N,CO]tts(g-t) as the GM, Table 3. Similar to K*Leu, this is in agreement with Lau et al. who reported Ile[CO,OH] as the GM at the B3LYP/6-311+G(3df,2p) level of theory. and Tsang et al. who also located this GM with the B3LYP/6-31G(d) level of theory (no Ile[CO] isomers listed). At 298 K, Ile[CO]cc(g-t) is identified as the GM and is more favored entropically than Ile[CO,OH]cc(g-t) by the B3LYP, B3P86, and B3LYP-Gd3BJ levels of theory, whereas Ile[CO,OH]cc(g-t) is identified as the GM by MP2. As seen with K*Leu at both temperatures, Ile[CO2]cc(g-t) is lower in energy than Ile[N,CO]tts(g-t) at the B3LYP, and B3P86 levels of theory, whereas Ile[CO2]cc(g-t) is lower in energy at the MP2 and B3LYP-GD3BJ levels of theory. The next lowest energy isomers are Ile[N,OH]tcs(g-t) followed by Ile[N]tt(tt).

Maxwellian equilibrium distributions at 298 K among Ile[CO]cc(g.t), Ile[CO,OH]cc(g.t), Ile[N,CO]tts(g.t), Ile[N,CO]tts(g.t), and Ile[CO₂-]cc(g.t) indicate that these species should comprise 47, 38, 2, 2, and 11% (B3LYP); 45, 40, 1, 1, and 13% (B3P86); and 30, 30, 22, 7, and 21% (B3LYP-GD3BJ), respectively. Again, the MP2 level predicts more of the [CO,OH] species with populations of 16, 40, 13, 5, and 13%, respectively.

Interconversion between [CO], [CO,OH], and [CO₂] Isomers. One of the difficulties in properly evaluating the [CO,OH] and [CO] isomers for all the amino acids considered here is that they lie in a double-well potential joined by allowing the K⁺ to swing around the carbonyl

group. In order to investigate this interconversion, we calculated the height of the TS barrier between the two isomers. With the exception of K⁺Gly, the TS universally lies below the [CO] isomer (by 0.5 - 1.6 kJ mol⁻¹ after ZPE corrections) for each system across all levels of theory indicating that the latter isomer collapses to the [CO,OH] isomer at 0 K, as illustrated in Figure 4 for the case of K⁺Ala. Ultimately, this means that the higher energy isomer is not truly stable, but it can be realized that ground and excited vibrational wavefunctions still sample both conformations, although the frequency of this vibration is unlikely to be accurately predicted by the harmonic approximations used here. In the case of K⁺Gly, the TS lies below the higher energy isomer for three levels of theory, but now the GM is [CO]cc at the B3LYP and B3P86 levels and [CO,OH]cc at the MP2 level. B3LYP-GD3BJ results are comparable to the MP2 results, but the TS lies 0.08 kJ mol⁻¹ above the higher energy [CO]cc isomer. In all cases, we view these doublewell potentials as having a vibrational wavefunction corresponding to potassium ion motion between the two isomers with a much higher amplitude in the [CO,OH]cc well. (For all complexes, Tables 1-3 also indicate that the energy of the TS between [CO,OH] and [CO] is much higher at 298 K, but this is a consequence of the thermal motion in all degrees of freedom and does not change the shape of the double-well potential.)

Furthermore, we also investigated the double-well potential between [CO,OH] and [CO₂⁻] isomers, corresponding to the motion of the proton between the hydroxy oxygen and amino nitrogen. Here, we have commented on similar behavior in a number of previous alkali metalated amino acids.^{27, 34, 40, 78} In all systems explored here, the [CO,OH] isomer is lower in energy at all levels of theory. For K⁺Gly, TS[CO,OH/CO₂⁻] lies 1.1 – 1.5 kJ mol⁻¹ *below* the [CO₂⁻]cc isomer for most levels of theory (5.7 kJ mol⁻¹ below at the B3P86 level), such that it should collapse to [CO,OH]cc. As the AA becomes larger, the energy of the [CO₂⁻] isomer decreases. Thus, for K⁺Ala, TS[CO,OH/CO₂⁻] is essentially isoenergetic with [CO₂⁻], as illustrated in Figure S2, and for larger AAs, TS[CO,OH/CO₂⁻] lies 0.6 – 2.0 kJ mol⁻¹ *above* [CO₂⁻] at most levels of theory. (B3P86 places the TS well below [CO₂⁻] for all K⁺AA.) In these cases, there is a true double-well potential with the vibrational wavefunction corresponding to the proton motion having a much

higher amplitude in the [CO,OH] well.

Threshold Analysis. Threshold regions of the zero-pressure extrapolated cross sections for Eq. 4 were analyzed using Eq. 1. In this analysis, PSL TSs for dissociation are assumed, such that the K^+AA GM complexes dissociate to form K^+ + GM neutral AAs. As noted above, this should be an adequate treatment of the TSs because the length of time available for dissociation is sufficient for each dissociating complex to completely explore phase space and reach its GM conformation upon dissociation. In all cases, the GM neutral AA ligands used in the analyses of the present study, Table 4, are the same as those discussed thoroughly in the study regarding Na $^+$ AA dissociation and agree with spectroscopic determinations of their conformations in previous studies. $^{95-104}$ In Figure 1, models are shown assuming the [CO,OH]cc reactant. Models assuming the K^+ AA[CO]cc reactant can be found in Supplementary Figure S1 and are very similar in all cases. As can be seen in Figure 1, these models reproduce the experimental data well from threshold up to 3-5 eV while also reproducing the entire cross section magnitudes over more than two orders of magnitude.

Because of the double-well potential that connects the [CO,OH]cc and [CO]cc isomers, we believe that there are potentially two reasonable interpretations of the data. i) Only the "stable" [CO,OH]cc isomer is considered to be populated. ii) Both isomers are considered with a population determined by an equilibrium distribution at 298 K. Given the average distributions calculated above for different levels of theory, this is essentially equivalent to taking the average of the two models for the three DFT approaches, whereas the MP2 results predict about a 2:1 ratio of [CO,OH]:[CO]. Contributions from the [CO₂⁻]cc isomers were considered to be negligible because the wavefunction corresponding to proton motion between the [CO₂⁻] and [CO,OH] potential wells should have little amplitude in the [CO₂⁻] well. For the heavier AAs, the [N,CO]tt_S isomers are also plausibly populated according to the B3LYP-GD3BJ level of theory; however, modeling with this reactant did not change the thresholds outside of the range of uncertainty listed.

Inspection of Table 4 reveals that the threshold for both [CO,OH] and [CO] GM reactants increases as the size of the side chain increases up to the K⁺hAla system, where it then stays

roughly the same well within the ranges of uncertainty. Notably, all of the fitting parameters between the [CO,OH] and [CO] reactants agree with each other (within uncertainty ranges) except for $\Delta S_{1000}^{\ddagger}$. The $\Delta S_{1000}^{\ddagger}$ values describe the degree of looseness for each dissociation reaction. All of the $\Delta S_{1000}^{\ddagger}$ values are positive, consistent with PSL reactions. For each system, the $\Delta S_{1000}^{\ddagger}$ values for the [CO,OH] reactant are higher than those for the [CO] reactant because movement of the K⁺ is more restricted in the bidentate [CO,OH] reactants than the monodentate [CO] reactants. As a result, there is more entropy gained by separating the K⁺ from the [CO,OH] reactants. Clearly, the distinction between the two thresholds in each system is small, lying within the absolute uncertainties of either value. As discussed above, our best interpretation of the data is either the [CO,OH]cc reactant values or an average of the [CO,OH]cc and [CO]cc values, but the distinction between these approaches is less than 0.01 eV. Further comparison with theory may provide additional insight into the most appropriate choice.

Conversion of Thermodynamic Parameters from 0 K to 298 K. Because there is often interest in thermodynamic information at room temperature, the conversion from 0 K thresholds to 298 K enthalpies and Gibbs energies is provided in Table 5. These values utilize the rigid rotor/harmonic oscillator approximation with rotational constants and vibrational frequencies calculated at the B3LYP/6-311+G(d,p) level for the [CO,OH]-cc(xx) and [CO]-cc(xx) reactants and ttt(xx) products. Uncertainties provided were determined by scaling the vibrational frequencies up and down by 10%. Such conversions may be limited by how accurate the low-frequency vibrational modes are. In particular, for the present cases, which all have alkyl groups except for glycine, the torsional vibrations of the methyl and perhaps higher-order alkyl groups may be better described as hindered rotors.

DISCUSSION

Theoretical Results for K⁺-AA Bond Dissociation Energies. Calculated using Eq. 3, BDEs at 0 K for each K⁺AA system are listed in Table 6 for the B3LYP, B3P86, MP2, and B3LYP-GD3BJ levels of theory both with and without BSSE corrections. Such calculations were made

under the assumption that each K⁺AA complex dissociates to the GM conformer of the AA product. When assuming a [CO,OH] reactant, the B3LYP and MP2 levels of theory consistently predict the lowest BDEs followed by the B3P86 and B3LYP-GD3BJ levels of theory, respectively; however, when assuming a [CO] reactant, the MP2 level of theory uniformly predicts the lowest BDEs followed by the B3LYP, B3P86, and B3LYP-GD3BJ levels of theory, respectively. This change occurs because the average excitation energy for the [CO] isomer for all six AA ligands is 1.8 ± 0.2 kJ mol⁻¹ at the three DFT levels of theory. For MP2, the [CO] isomer lies 2.6 - 5.8 kJ/mol above [CO,OH]. When including BSSE corrections, there are no significant changes in results for the B3LYP, B3P86, and B3LYP-GD3BJ levels of theory (differences are < 1 kJ mol⁻¹); however, BSSE corrections at the MP2 level of theory consistently lower the BDE by ~ 4 kJ mol⁻¹ for both reactant isomers, Table 6. Comparable counterpoise corrections were found for Na⁺-AA BDEs for the same set of AA ligands.⁷⁸

Experiment Versus Theory. To compare the 0 K experimental and theoretical BDEs for each K⁺AA system, we first average the experimental results for the [CO,OH] and [CO] reactants. As noted above, this is probably our best overall interpretation of the present results. For the theoretical values, we likewise average the predicted 0 K BDEs for the [CO,OH] and [CO] isomers (essentially the 298 K distribution for the three DFT levels of theory), but for MP2, we take a 2:1 mixture of the [CO,OH]:[CO] results, again reflecting the predicted 298 K Maxwellian distribution. These averaged values are compared in Table 6.

The present TCID measurement for K⁺Gly agrees well with the values of $121 \pm 4 \text{ kJ mol}^{-1}$ from prior GIBMS experiments of Moision and Armentrout²⁴ and with $125 \pm 10 \text{ kJ mol}^{-1}$ from triple quad experiments of Klassen et al.,¹⁰⁹ falling well within experimental uncertainty of either measurement. The drop from our previous study, 121 ± 4 to $118.3 \pm 4.2 \text{ kJ/mol}$, is partially attributed to including the [CO] reactant (which has a lower threshold energy) in the present interpretation, whereas only the [CO,OH] reactant was included previously. Further, the present data was analyzed over a longer energy range, which led to a slightly higher value of n (1.0 ± 0.1) compared with previously (0.94 ± 0.02), which will decrease the E_0 value. Finally, careful

examination of the previous data indicates that the model falls slightly below the experimental data in the threshold region, consistent with the need for a slightly lower threshold.

Generally, the B3LYP results (both with and without BSSE corrections) agree well with the TCID values for each reactant, with a mean absolute deviation (MAD) of about 1 kJ mol⁻¹. Likewise, MP2 results without BSSE agree very well (MAD of 1.5 kJ mol⁻¹), but the counterpoise corrections systematically drop the predicted values below experiment, yielding a MAD of ~6 kJ mol⁻¹. B3P86 both with and without BSSE has a MAD near 2 kJ mol⁻¹. In contrast, the B3LYP-GD3BJ level of theory (with and without BSSE corrections) consistently overestimates the BDEs for both reactants by 5-9 kJ mol⁻¹. If specific experimental and theoretical BDEs for the [CO,OH] or [CO] reactants are compared directly instead of the averages provided in Table 6, the overall results are qualitatively similar (within 1 kJ mol⁻¹), except MP2 results are better for [CO,OH] $(MAD = 1.0 \pm 0.9 \text{ kJ mol}^{-1})$ and worse for [CO] $(MAD = 3.9 \pm 1.4 \text{ kJ mol}^{-1})$. Overall, considering an average experimental uncertainty of 5 kJ mol⁻¹, B3LYP, B3P86, and MP2 approaches predict BDEs in good agreement with our experimental values, whereas adding dispersion to B3LYP overbinds. Considering these are non-covalent complexes, the latter finding is somewhat surprising but was also found for the sodiated analogues (as discussed further below). Further, the discrepancy noted here is comparable to the overbinding found for alkali cation (Li⁺, Na⁺, K⁺) benzene complexes used in the development of the improved GD3 dispersion corrections.⁹¹

Theory consistently indicates that Val binds more tightly to K^+ than hAla, by an average of 1.4 ± 0.4 kJ mol⁻¹, whereas our experimental result indicates the opposite by 0.7 kJ mol⁻¹, although both differences are well within the absolute uncertainty of either value. In addition, all levels of theory indicate that K^+ binds slightly more strongly to Ile (by 1.0 ± 0.4 kJ mol⁻¹) than to the isobaric Leu. When the data is interpreted using the [CO,OH] reactant, this result is also obtained, with a difference measured of 0.5 kJ mol⁻¹, whereas assuming a [CO] reactant yields the opposite result by 1.9 kJ mol⁻¹, such that the average difference listed in Table 6 is 0.7 kJ/mol. Again these differences are well within the uncertainties of either experimental BDE, but suggest that the double-well potential should be biased towards [CO,OH].

Comparisons to the Kinetic Method. The KM results from Tsang et al.⁵² are the only other experimental BDEs reported for these systems other than K $^+$ Gly, Table 6. In their study, absolute K $^+$ affinities were assigned using theoretical values for the reference molecules acetamide, N-methylacetamide, and N,N-dimethylacetamide. Their results are in good agreement with the present TCID results, although their values are systematically higher with a MAD of 2 \pm 1 kJ mol $^{-1}$, well within the uncertainties of either measurement. If comparisons are made to the individual results we obtain assuming either a [CO,OH] or [CO] reactant, then the MADs change to 1 \pm 1 and 3 \pm 2 kJ mol $^{-1}$, respectively, perhaps again suggesting a bias towards the [CO,OH] species. If the KM values are reanchored to the present experimental results by shifting down by 2 kJ mol $^{-1}$, the MAD drops to 0.8 ± 0.5 kJ mol $^{-1}$ when comparing the KM results to the average threshold values here. Overall, we take these comparisons to indicate that using the average threshold values is appropriate for these systems and that a bias toward enhanced [CO,OH] population should be considered.

Previously, Hoyau and Ohanessian¹⁰⁵ and Rožman¹¹⁰ have pointed out that the KM can only produce accurate thermodynamic information on the true GM of a M⁺AA complex if the (AA₁)M⁺(AA₂) heterodimer used has the same binding mode as M⁺(AA₁) and M⁺(AA₂) products. This is required because there is generally not adequate time for the complex to reorganize during dissociation. For potassiated heterodimers, we think this difficulty may not be a complication as the "end-on" binding mode associated with the [CO,OH] and [CO] isomers (as well as the reference acetamides) means there is probably little steric interference between the two ligands in the heterodimer. Although there is a potential complication in having both [CO,OH] and [CO] isomers populated, because these actually occupy a single double-well potential, rearrangement between these forms should be facile even under KM conditions. As a result, the relative KM values are in agreement with the present absolute BDEs (certainly within the generous uncertainties of the KM results).

Bond Dissociation Energy Trends. Inspection of both experimental and theoretical BDEs, Table 6, indicate that increasing AA size generally increases the stability of the K⁺AA

complex. The one exception is K⁺hAla, which has a slightly higher experimental BDE than K⁺Val. Notably, these two values are not distinguishable outside the ranges of uncertainty, so it is possible that the K⁺hAla BDE is actually lower than that for K⁺Val.

This general trend in the BDEs as a function of side chain length can be appreciated more quantitatively by considering the effect of the polarizability (α) of the AA. Figure 5 shows the averaged K⁺AA BDEs of Table 6 plotted as a function of polarizability. Here, the polarizabilities are taken from experimental results in solution,¹¹¹ except for hAla, which was taken as the average of Ala and Val. The data is clearly very linear such that a linear regression analysis of the data finds that BDE (kJ mol⁻¹) = 111.9 ± 6.4 + (1.10 ± 0.58) α (R^2 = 0.90). If the hAla data point is excluded, the analysis changes only slightly to BDE = 111.1 ± 7.5 + (1.14 ± 0.66) α (R^2 = 0.99), but the plot is more linear. A linear trend is also seen when using the theoretical BDEs or the BDEs obtained from the KM.

In addition to the overall trend with changing aliphatic AA, the relative energies of different isomers can be examined using the theoretical results. For Gly, the [CO,OH] and [CO] isomers are nearly isoenergetic with the [CO] isomer increasing in energy with the size of the AA to reach an excitation energy of about 2-6 kJ mol⁻¹ for Val, Leu, and Ile, Tables 1-3. In contrast, theoretical calculations indicate that the [CO₂⁻] ZW isomer becomes more energetically favorable as the AA side chain size increases, Tables 1-3. Starting at an excitation energy of 9-12 kJ mol⁻¹ for Gly, this decreases to 2-3 kJ mol⁻¹ for Val and Ile (with Leu about 1 kJ mol⁻¹ higher). Both of these general trends likely result from the increased polarizability, which helps stabilize the bidentate coordination and enhances the proton transfer needed to yield the zwitterionic AA. Notably, the [CO,OH] isomer still dominates for all AA. The alternative [N,CO] isomer has an excitation energy that changes little with changing AA, but varies considerably among the levels of theory, with excitation energies of 4-6 kJ mol⁻¹ for B3LYP, 6-9 kJ mol⁻¹ for B3P86, 2-3 kJ mol⁻¹ for MP2, and 0-1 kJ mol⁻¹ for B3LYP-GD3BJ. As noted above, this latter level of theory does not reproduce the experimental BDEs very well (Table 6) and if the predicted [N,CO] GM were used to calculate the B3LYP-GD3BJ BDEs, the deviations would be worse (increasing by about 2 kJ

mol⁻¹).

Comparisons to Sodium Cation Complexes. As for all ligands, 112-113 the smaller, higher charge density Na⁺ cation binds more tightly to the AAs than K⁺. The BDE trend is similar for both systems as it increases with AA size and polarizability. 78 Indeed, the K+AA BDEs measured here are uniformly $73 \pm 1\%$ of the Na⁺AA BDEs. This is similar to the trends observed for other amino acids with functionalized side chains where a $74 \pm 3\%$ ratio has been noted. 113 Notably, the largest deviation from this ratio occurs for AA = hAla because the K⁺hAla BDE is relatively high and the Na⁺hAla BDE is relatively low compared to the linear regression analysis. This observation simply documents that the high experimental value of the K⁺hAla BDE is not a systematic result. We can also compare the success of different levels of theory in predicting the BDEs of the Na⁺AA and K⁺AA complexes. As found here, the B3LYP and B3P86 levels (with and without BSSE) performed reasonably well as did MP2 without BSSE. For the Na⁺AA analogues, the MAD was 2 \pm 1 kJ mol⁻¹ with no BSSE and 11 \pm 1 kJ mol⁻¹ (systematically low) including counterpoise corrections, ⁷⁸ comparable to the effect seen here when including BSSE corrections to the MP2 results. Likewise, as for the potassiated analogues, B3LYP-GD3BJ calculations for the Na⁺AA complexes were systematically high, by 14 ± 3 kJ mol⁻¹ including counterpoise corrections. In the Na⁺AA work, M06-2X¹¹⁴ calculations were also performed, but also gave systematically high results, with a MAD of 7 ± 3 kJ mol⁻¹ including BSSE corrections, and therefore this level of theory was not pursued here.

CONCLUSIONS

Bond dissociation energies of K^+AA (AA = Gly, Ala, hAla, Val, Leu, and Ile) were measured via kinetic-energy-dependent TCID studies with Xe using a GIBMS. In each case, the loss of the neutral ligand is the only process observed. Theoretical calculations suggest that both [CO,OH] and [CO] reactants are present, coupled together in an asymmetric double-well potential, and that there are weak interactions between K^+ and the alkyl side chains. Experimental K^+AA BDEs at 0 K adopt the following trend: $K^+Gly < K^+Ala < K^+Val \approx K^+hAla < K^+Leu \approx K^+Ile$, when

the data are analyzed assuming either a [CO,OH] or [CO] reactant. Because of the double-well potentials for the global minima, we believe that our best evaluation of the K⁺AA BDEs is an average of the [CO,OH] and [CO] threshold values, which differ only slightly from one another. Theoretical calculations and the KM indicate that the BDE for K⁺Ile is greater than that for K⁺Leu and that the BDE for K⁺Val is greater than that of K⁺hAla, whereas the present average experimental results predict the opposite, although the disagreements are well within the uncertainties. The overall trend in the K⁺AA BDEs measured here can be explained by the increasing polarizabilities of the AAs as the side chain length increases. Generally, the B3LYP, B3P86, and MP2 (without counterpoise corrections) levels of theory agree well with experimental results, whereas the B3LYP-GD3BJ level of theory consistently overestimates the values.

ASSOCIATED CONTENT

Supporting Information

The Supporting Information is available free of charge at https://pubs.aco.org/doi/10.1021/jasms.xxxx

Tables of relative 0 K enthalpies and 298 K Gibbs energies of high-energy potassiated Gly, Ala, hAla, Val, Leu, and Ile complexes calculated at several levels of theory. Figure showing the cross sections analysis assuming a [CO] reactant. Figure showing the double well potential for K+Ala[CO,OH]cc and K+Ala[CO2–]cc. Figures showing the lowest energy structures of potassiated Gly, hAla, Val, Leu, and Ile calculated at the B3LYP/6-311+G(d,p) level.

AUTHOR INFORMATION

Corresponding Author

P. B. Armentrout - orcid.org/0000-0003-2953-6039; Email: armentrout@chem.utah.edu

Notes

The authors declare no competing financial interest.

ACKNOWLEDGMENTS

The authors acknowledge support for this study by the National Science Foundation, Grant CHE-1954142 and a grant of computer time from the Center for High Performance Computing at the University of Utah.

REFERENCES

- 1. Garlid, K. D., Cation transport in mitochondria The potassium cycle. *Biochim Biophys Acta Bioenerg* **1996**, *1275*, 123-126.
- 2. Bortner, C. D.; Cidlowski, J. A., Cell shrinkage and monovalent cation fluxes: Role in apoptosis. *Arch. Biochem. Biophys.* **2007**, *462*, 176-188.
- 3. Jaiswal, D. K.; Verma, J. P.; Prakash, S.; Meena, V. S.; Meena, R. S., Potassium as an Important Plant Nutrient in Sustainable Agriculture: A State of the Art. In *Potassium Solubilizing Microorganisms for Sustainable Agriculture*, 2016; pp 21-29.
- 4. Lutsenko, S.; Kaplan, J. H., An Essential Role for the Extracellular Domain of the Na,K-ATPase β-Subunit in Cation Occlusion. *Biochem* **1993**, *32*, 6737-6743.
- 5. Thomas, R. C., Electrogenic sodium pump in nerve and muscle cells. *Physiol. Rev.* **1972**, 52, 563-594.
- 6. Beeler Jr, G. W.; Reuter, H., Voltage clamp experiments on ventricular myocardial fibres. *J. Physiol.* **1970**, *207*, 165-190.
- 7. Stockklausner, C.; Klöcker, N., Surface Expression of Inward Rectifier Potassium Channels Is Controlled by Selective Golgi Export. *J. Biol. Chem.* **2003**, *278*, 17000-17005.
- 8. Akao, M.; Ohler, A.; O'Rourke, B.; Marbán, E., Mitochondrial ATP-Sensitive Potassium Channels Inhibit Apoptosis Induced by Oxidative Stress in Cardiac Cells. *Circ. Res.* **2001,** *88*, 1267-1275.
- 9. Bengoechea, J. A.; Skurnik, M., Temperature-regulated efflux pump/potassium antiporter

- system mediates resistance to cationic antimicrobial peptides in Yersinia. *Mol. Microbiol.* **2000**, *37*, 67-80.
- 10. Shealy, R. T.; Murphy, A. D.; Ramarathnam, R.; Jakobsson, E.; Subramaniam, S., Sequence-function analysis of the K⁺-selective family of ion channels using a comprehensive alignment and the KcsA channel structure. *Biophys. J.* **2003**, *84*, 2929-2942.
- 11. Heginbotham, L.; Lu, Z.; Abramson, T.; MacKinnon, R., Mutations in the K⁺ channel signature sequence. *Biophys. J.* **1994**, *66*, 1061-1067.
- 12. Rodgers, M. T.; Armentrout, P. B., A Thermodynamic "Vocabulary" for Metal Ion Interactions in Biological Systems. *Acc. Chem. Res.* **2004**, *37*, 989-998.
- 13. Neher, E.; Sakmann, B.; Steinbach, J. H., The extracellular patch clamp: A method for resolving currents through individual open channels in biological membranes. *Pflügers Archiv* **1978**, *375*, 219-228.
- 14. Eyring, H., The Activated Complex in Chemical Reactions. *J. Chem. Phys.* **1935**, *3*, 107-115.
- 15. Eyring, H., The Activated Complex and the Absolute Rate of Chemical Reactions. *Chem. Rev.* **1935,** *17*, 65-77.
- 16. Sigg, D., Modeling ion channels: past, present, and future. J Gen Physiol 2014, 144, 7-26.
- 17. Blachly-Dyson, E.; Peng, S.; Colombini, M.; Forte, M., Selectivity changes in site-directed mutants of the VDAC ion channel: structural implications. *Science* **1990**, *247*, 1233.
- 18. Yoshimura, K.; Batiza, A.; Schroeder, M.; Blount, P.; Kung, C., Hydrophilicity of a Single Residue within MscL Correlates with Increased Channel Mechanosensitivity. *Biophys. J.* **1999**, 77, 1960-1972.
- 19. Hilf, R. J. C.; Dutzler, R., Structure of a potentially open state of a proton-activated pentameric ligand-gated ion channel. *Nature* **2009**, *457*, 115-118.
- 20. Kashiwagi, K.; Masuko, T.; Nguyen, C. D.; Kuno, T.; Tanaka, I.; Igarashi, K.; Williams, K., Channel Blockers Acting at N-Methyl-D-aspartate Receptors: Differential Effects of Mutations in the Vestibule and Ion Channel Pore. *Mol. Pharmacol.* **2002**, *61*, 533.

- 21. Kirsch, G. E.; Drewe, J. A.; Taglialatela, M.; Joho, R. H.; DeBiasi, M.; Hartmann, H. A.; Brown, A. M., A single nonpolar residue in the deep pore of related K+ channels acts as a K+:Rb+ conductance switch. *Biophys. J.* **1992**, *62*, 136-144.
- 22. Doyle, D. A.; Cabral, J. M.; Pfuetzner, R. A.; Kuo, A.; Gulbis, J. M.; Cohen, S. L.; Chait, B. T.; MacKinnon, R., The Structure of the Potassium Channel: Molecular Basis of K+ Conduction and Selectivity. *Science* **1998**, *280*, 69.
- 23. Heginbotham, L.; Abramson, T.; MacKinnon, R., A functional connection between the pores of distantly related ion channels as revealed by mutant K⁺ channels. *Science* **1992**, *258*, 1152.
- 24. Moision, R. M.; Armentrout, P. B., An experimental and theoretical dissection of potassium cation/glycine interactions. *Phys. Chem. Chem. Phys.* **2004**, *6*, 2588-2599.
- 25. Heaton, A. L.; Armentrout, P. B., Experimental and Theoretical Studies of Potassium Cation Interactions with the Acidic Amino Acids and Their Amide Derivatives. *J. Phys. Chem. B* **2008**, *112*, 12056-12065.
- 26. Mookherjee, A.; Armentrout, P. B., Theoretical investigation and reinterpretation of the decomposition of lithiated proline and N-methyl proline. *Int. J. Mass Spectrom.* **2014**, *370*, 16-28.
- 27. Clark, A. A.; Yang, B.; Rodgers, M. T.; Armentrout, P. B., Experimental and Computational Study of the Group 1 Metal Cation Chelates with Lysine: Bond Dissociation Energies, Structures, and Structural Trends. *J. Phys. Chem. B.* **2019**, *123*, 1983-1997.
- 28. Moision, R. M.; Armentrout, P. B., Experimental and Theoretical Dissection of Sodium Cation/Glycine Interactions. *J. Phys. Chem. A.* **2002**, *106*, 10350-10362.
- 29. Heaton, A. L.; Moision, R. M.; Armentrout, P. B., Experimental and Theoretical Studies of Sodium Cation Interactions with the Acidic Amino Acids and Their Amide Derivatives. *J. Phys. Chem. A* **2008**, *112*, 3319-3327.
- 30. Rodgers, M. T.; Armentrout, P. B., Noncovalent Interactions of Nucleic Acid Bases (Uracil, Thymine, and Adenine) with Alkali Metal Ions. Threshold Collision-Induced Dissociation and Theoretical Studies. *J. Am. Chem. Soc.* **2000**, *122*, 8548-8558.
- 31. Ruan, C.; Rodgers, M. T., Cation- π Interactions: Structures and Energetics of

- Complexation of Na⁺ and K⁺ with the Aromatic Amino Acids, Phenylalanine, Tyrosine, and Tryptophan. *J. Am. Chem. Soc.* **2004**, *126*, 14600-14610.
- 32. Carl, D. R.; Cooper, T. E.; Oomens, J.; Steill, J. D.; Armentrout, P. B., Infrared multiple photon dissociation spectroscopy of cationized methionine: effects of alkali-metal cation size on gas-phase conformation. *Phys. Chem. Chem. Phys.* **2010**, *12*, 3384-3398.
- 33. Armentrout, P. B.; Rodgers, M. T.; Oomens, J.; Steill, J. D., Infrared Multiphoton Dissociation Spectroscopy of Cationized Serine: Effects of Alkali-Metal Cation Size on Gas-Phase Conformation. *J. Phys. Chem. A.* **2008**, *112*, 2248-2257.
- 34. Rodgers, M. T.; Armentrout, P. B.; Oomens, J.; Steill, J. D., Infrared Multiphoton Dissociation Spectroscopy of Cationized Threonine: Effects of Alkali-Metal Cation Size on Gas-Phase Conformation. *J. Phys. Chem. A.* **2008**, *112*, 2258-2267.
- 35. Citir, M.; Stennett, E. M. S.; Oomens, J.; Steill, J. D.; Rodgers, M. T.; Armentrout, P. B., Infrared multiple photon dissociation spectroscopy of cationized cysteine: Effects of metal cation size on gas-phase conformation. *Int. J. Mass Spectrom.* **2010**, *297*, 9-17.
- 36. Polfer, N. C.; Oomens, J.; Dunbar, R. C., IRMPD spectroscopy of metal-ion/tryptophan complexes. *Phys. Chem. Chem. Phys.* **2006**, *8*, 2744-2751.
- 37. Forbes, M. W.; Bush, M. F.; Polfer, N. C.; Oomens, J.; Dunbar, R. C.; Williams, E. R.; Jockusch, R. A., Infrared Spectroscopy of Arginine Cation Complexes: Direct Observation of Gas-Phase Zwitterions. *J. Phys. Chem. A.* **2007**, *111*, 11759-11770.
- 38. O'Brien, J. T.; Prell, J. S.; Steill, J. D.; Oomens, J.; Williams, E. R., Interactions of Monoand Divalent Metal Ions with Aspartic and Glutamic Acid Investigated with IR Photodissociation Spectroscopy and Theory. *J. Phys. Chem. A.* **2008**, *112*, 10823-10830.
- 39. Heaton, A. L.; Bowman, V. N.; Oomens, J.; Steill, J. D.; Armentrout, P. B., Infrared Multiple Photon Dissociation Spectroscopy of Cationized Asparagine: Effects of Metal Cation Size on Gas-Phase Conformation. *J. Phys. Chem. A.* **2009**, *113*, 5519-5530.
- 40. Citir, M.; Hinton, C. S.; Oomens, J.; Steill, J. D.; Armentrout, P. B., Infrared Multiple Photon Dissociation Spectroscopy of Cationized Histidine: Effects of Metal Cation Size on Gas-

- Phase Conformation. J. Phys. Chem. A. 2012, 116, 1532-1541.
- 41. Armentrout, P. B.; Armentrout, E. I.; Clark, A. A.; Cooper, T. E.; Stennett, E. M. S.; Carl, D. R., An Experimental and Theoretical Study of Alkali Metal Cation Interactions with Cysteine. *J. Phys. Chem. B.* **2010**, *114*, 3927-3937.
- 42. Armentrout, P. B.; Gabriel, A.; Moision, R. M., An experimental and theoretical study of alkali metal cation/methionine interactions. *Int. J. Mass Spectrom.* **2009**, *283*, 56-68.
- 43. Grese, R. P.; Cerny, R. L.; Gross, M. L., Metal ion-peptide interactions in the gas phase: a tandem mass spectrometry study of alkali metal cationized peptides. *J. Am. Chem. Soc.* **1989**, *111*, 2835-2842.
- 44. Polfer, N. C.; Oomens, J., Vibrational spectroscopy of bare and solvated ionic complexes of biological relevance. *Mass Spectrom. Rev.* **2009**, *28*, 468-494.
- 45. Wyttenbach, T.; Witt, M.; Bowers, M. T., On the question of salt bridges of cationized amino acids in the gas phase: glycine and arginine *Int. J. Mass Spectrom.* **1999**, *182-183*, 243-252.
- 46. Armentrout, P. B.; Citir, M.; Chen, Y.; Rodgers, M. T., Thermochemistry of Alkali Metal Cation Interactions with Histidine: Influence of the Side Chain. *J. Phys. Chem. A.* **2012**, *116*, 11823-11832.
- 47. Drayß, M. K.; Armentrout, P. B.; Oomens, J.; Schäfer, M., IR spectroscopy of cationized aliphatic amino acids: Stability of charge-solvated structure increases with metal cation size. *Int. J. Mass Spectrom.* **2010**, *297*, 18-27.
- 48. Drayss, M. K.; Blunk, D.; Oomens, J.; Schäfer, M., Infrared Multiple Photon Dissociation Spectroscopy of Potassiated Proline. *J. Phys. Chem. A.* **2008**, *112*, 11972-11974.
- Drayβ, M. K.; Blunk, D.; Oomens, J.; Gao, B.; Wyttenbach, T.; Bowers, M. T.; Schäfer, M., Systematic Study of the Structures of Potassiated Tertiary Amino Acids: Salt Bridge Structures Dominate. J. Phys. Chem. A. 2009, 113, 9543-9550.
- 50. Rodgers, M. T.; Armentrout, P. B., Cationic Noncovalent Interactions: Energetics and Periodic Trends. *Chem. Rev.* **2016**, *116*, 5642-5687.
- 51. McLuckey, S. A.; Cameron, D.; Cooks, R. G., Proton affinities from dissociations of

- proton-bound dimers. J. Am. Chem. Soc. 1981, 103, 1313-1317.
- 52. Tsang, Y.; Wong, C. C. L.; Wong, C. H. S.; Cheng, J. M. K.; Ma, N. L.; Tsang, C. W., Proton and potassium affinities of aliphatic and N-methylated aliphatic α-amino acids: Effect of alkyl chain length on relative stabilities of K⁺ bound zwitterionic complexes. *Int. J. Mass Spectrom.* **2012**, *316-318*, 273-283.
- 53. Marino, T.; Russo, N.; Toscano, M., Potential Energy Surfaces for the Gas-Phase Interaction between α-Alanine and Alkali Metal Ions (Li⁺, Na⁺, K⁺). A Density Functional Study. *Inorg. Chem.* **2001**, *40*, 6439-6443.
- 54. Lau, J. K.-C.; Wong, C. H. S.; Ng, P. S.; Siu, F. M.; Ma, N. L.; Tsang, C. W., Absolute Potassium Cation Affinities (PCAs) in the Gas Phase. *Chem. Eur. J.* **2003**, *9*, 3383-3396.
- 55. Wong, C. H. S.; Siu, F. M.; Ma, N. L.; Tsang, C. W., A theoretical study of potassium cation-glycine (K⁺-Gly) interactions. *J. Molec. Struct. THEOCHEM* **2002**, *588*, 9-16.
- 56. Amicangelo, J. C.; Armentrout, P. B., Relative and absolute bond dissociation energies of sodium cation complexes determined using competitive collision-induced dissociation experiments. *Int. J. Mass Spectrom.* **2001**, *212*, 301-325.
- 57. Amicangelo, J. C.; Armentrout, P. B., Absolute Binding Energies of Alkali-Metal Cation Complexes with Benzene Determined by Threshold Collision-Induced Dissociation Experiments and ab Initio Theory. *J. Phys. Chem. A.* **2000**, *104*, 11420-11432.
- 58. Rodgers, M. T.; Armentrout, P. B., Collision-Induced Dissociation Measurements on $Li^+(H_2O)_n$, n = 1-6: The First Direct Measurement of the Li^+-OH_2 Bond Energy. *J. Phys. Chem. A.* **1997**, *101*, 1238-1249.
- 59. Rodgers, M. T.; Armentrout, P. B., Noncovalent metal–ligand bond energies as studied by threshold collision-induced dissociation. *Mass Spectrom. Rev.* **2000**, *19*, 215-247.
- 60. Ervin, K. M.; Armentrout, P. B., Translational energy dependence of $Ar^++XY \rightarrow ArX^++Y$ (XY=H₂,D₂,HD) from thermal to 30 eV c.m. *J. Chem. Phys.* **1985**, *83*, 166-189.
- 61. Armentrout, P. B., Mass spectrometry—not just a structural tool: the use of guided ion beam tandem mass spectrometry to determine thermochemistry. *J. Am. Soc. Mass. Spectrom.* **2002**,

- 13, 419-434.
- 62. Muntean, F.; Armentrout, P. B., Guided ion beam study of collision-induced dissociation dynamics: integral and differential cross sections. *J. Chem. Phys.* **2001**, *115*, 1213-1228.
- 63. Moision, R. M.; Armentrout, P. B., An electrospray ionization source for thermochemical investigation with the guided ion beam mass spectrometer. *J. Am. Soc. Mass. Spectrom.* **2007**, *18*, 1124-1134.
- 64. Kim, T.; Tolmachev, A. V.; Harkewicz, R.; Prior, D. C.; Anderson, G.; Udseth, H. R.; Smith, R. D.; Bailey, T. H.; Rakov, S.; Futrell, J. H., Design and Implementation of a New Electrodynamic Ion Funnel. *Anal. Chem.* **2000**, *72*, 2247-2255.
- 65. Mookherjee, A.; Van Stipdonk, M. J.; Armentrout, P. B., Thermodynamics and Reaction Mechanisms of Decomposition of the Simplest Protonated Tripeptide, Triglycine: A Guided Ion Beam and Computational Study. *J. Am. Soc. Mass. Spectrom.* **2017**, *28*, 739-757.
- 66. Armentrout, P. B.; Heaton, A. L., Thermodynamics and Mechanisms of Protonated Diglycine Decomposition: A Guided Ion Beam Study. *J. Am. Soc. Mass. Spectrom.* **2012**, *23*, 632-643.
- 67. Ye, S. J.; Armentrout, P. B., Absolute Thermodynamic Measurements of Alkali Metal Cation Interactions with a Simple Dipeptide and Tripeptide. *J. Phys. Chem. A* **2008**, *112*, 3587-3596.
- 68. Ye, S. J.; Clark, A. A.; Armentrout, P. B., Experimental and Theoretical Investigation of Alkali Metal Cation Interactions with Hydroxyl Side-Chain Amino Acids. *J. Phys. Chem. B* **2008**, *112*, 10291-10302.
- 69. Carl, D. R.; Chatterjee, B. K.; Armentrout, P. B., Threshold collision-induced dissociation of $Sr^{2+}(H_2O)_x$ complexes (x=1-6): An experimental and theoretical investigation of the complete inner shell hydration energies of Sr^{2+} . *J. Chem. Phys.* **2010**, *132*, 044303.
- 70. Jones, R. M.; Boles, G. C.; Armentrout, P. B., Cis-trans isomerization is not rate determining for b₂ ion structures: A guided ion beam and computational study of the decomposition of H⁺(GlyProAla). *Int. J. Mass Spectrom.* **2020**, *458*, 116434.

- 71. Mookherjee, A.; Armentrout, P. B., Thermodynamics and Reaction Mechanisms for Decomposition of a Simple Protonated Tripeptide, H⁺GAG: a Guided Ion Beam and Computational Study. *J. Am. Soc. Mass. Spectrom.* **2019**, *30*, 1013-1027.
- 72. Teloy, E.; Gerlich, D., Integral cross sections for ion—molecule reactions. I. The guided beam technique. *Chem. Phys.* **1974**, *4*, 417-427.
- 73. Gerlich, D., Inhomogeneous RF Fields: A Versatile Tool for the Study of Processes with Slow Ions. In *Adv. Chem. Phys.*, 1992; Vol. 82, pp 1-176.
- 74. Daly, N. R., Scintillation Type Mass Spectrometer Ion Detector. *Rev. Sci. Instrum.* **1960**, 31, 264-267.
- 75. Rodgers, M. T.; Ervin, K. M.; Armentrout, P. B., Statistical modeling of collision-induced dissociation thresholds. *J. Chem. Phys.* **1997**, *106*, 4499-4508.
- 76. Rodgers, M. T.; Armentrout, P. B., Statistical modeling of competitive threshold collision-induced dissociation. *J. Chem. Phys.* **1998**, *109*, 1787-1800.
- 77. Armentrout, P. B., Statistical modeling of sequential collision-induced dissociation thresholds. *J. Chem. Phys.* **2007**, *126*, 234302.
- 78. Pham, H. D. M.; Boles, G. C.; Armentrout, P. B., Sodium Binding Interactions with Aliphatic Amino Acids: A Guided Ion Beam and Computational Study. *J. Phys. Chem. A.* **2021**, *125*, 6332-6347.
- 79. Gilbert, R. G.; Smith, S. C., *Theory of unimolecular and recombination reactions*. Blackwell Scientific: London, 1990.
- 80. Robinson, P. J.; Holbrook, K. A., *Unimolecular reactions*. Wiley Interscience: New York, 1972.
- 81. Beyer, T.; Swinehart, D. F., Algorithm 448: number of multiply-restricted partitions. *Commun. ACM* **1973**, *16*, 379.
- 82. Stein, S. E.; Rabinovitch, B. S., Accurate evaluation of internal energy level sums and densities including anharmonic oscillators and hindered rotors. *J. Chem. Phys.* **1973**, *58*, 2438-2445.

- 83. Stein, S. E.; Rabinovitch, B. S., On the use of exact state counting methods in RRKM rate calculations. *Chem. Phys. Lett.* **1977**, *49*, 183-188.
- 84. Hales, D. A.; Lian, L.; Armentrout, P. B., Collision-induced dissociation of Nb^{+ n} (n = 2 11): bond energies and dissociation pathways. *Int. J. Mass Spectrom. Ion Processes* **1990**, *102*, 269-301.
- 85. Tiernan, O., Kinetic Shifts. Eur. J. Mass Spectrom. 2002, 8, 85-98.
- 86. Case, D.; Babin, V.; Berryman, J.; Betz, R.; Cai, Q.; Cerutti, D.; Cheatham, T.; Darden, T.; Duke, R.; Gohlke, H.; Götz, A.; Gusarov, S.; Homeyer, N.; Janowski, P.; Kaus, J.; Kolossváry, I.; Kovalenko, A.; Lee, T.-S.; Legrand, S.; Kollman, P., *Amber 2014*. 2014.
- 87. Schlegel, H. B., Optimization of equilibrium geometries and transition structures. *J. Comput. Chem.* **1982**, *3*, 214-218.
- 88. Lee, C.; Yang, W.; Parr, R. G., Development of the Colle-Salvetti correlation-energy formula into a functional of the electron density. *Phys. Rev. B* **1988**, *37*, 785-789.
- 89. Hehre, W. J., Ab initio molecular orbital theory. Acc. Chem. Res. 1976, 9, 399-406.
- 90. Montgomery, J. A.; Frisch, M. J.; Ochterski, J. W.; Petersson, G. A., A complete basis set model chemistry. VI. Use of density functional geometries and frequencies. *J. Chem. Phys.* **1999**, *110*, 2822-2827.
- 91. Grimme, S.; Antony, J.; Ehrlich, S.; Krieg, H., A consistent and accurate ab initio parametrization of density functional dispersion correction (DFT-D) for the 94 elements H-Pu. *J. Chem. Phys.* **2010**, *132*, 154104.
- 92. Grimme, S.; Ehrlich, S.; Goerigk, L., Effect of the damping function in dispersion corrected density functional theory. *J. Comput. Chem.* **2011**, *32*, 1456-1465.
- 93. Mookherjee, A.; Armentrout, P. B., Role of methylation on the thermochemistry of alkali metal cation complexes of amino acids: N-methyl proline. *Int. J. Mass Spectrom.* **2013**, *345-347*, 109-119.
- 94. Boys, S. F.; Bernardi, F., The calculation of small molecular interactions by the differences of separate total energies. Some procedures with reduced errors. *Mol. Phys.* **1970**, *19*, 553-566.

- 95. Stepanian, S. G.; Reva, I. D.; Radchenko, E. D.; Rosado, M. T. S.; Duarte, M. L. T. S.; Fausto, R.; Adamowicz, L., Matrix-Isolation Infrared and Theoretical Studies of the Glycine Conformers. *J. Phys. Chem. A.* **1998**, *102*, 1041-1054.
- 96. Ivanov, A. Y.; Sheina, G.; Blagoi, Y. P., FTIR spectroscopic study of the UV-induced rotamerization of glycine in the low temperature matrices (Kr, Ar, Ne). *Spectrochim. Acta A Mol. Biomol. Spectrosc.* **1998,** *55*, 219-228.
- 97. Blanco, S.; Lesarri, A.; López, J. C.; Alonso, J. L., The Gas-Phase Structure of Alanine. *J. Am. Chem. Soc.* **2004**, *126*, 11675-11683.
- 98. Stepanian, S. G.; Reva, I. D.; Radchenko, E. D.; Adamowicz, L., Conformational Behavior of α-Alanine. Matrix-Isolation Infrared and Theoretical DFT and ab Initio Study. *J. Phys. Chem. A.* **1998,** *102*, 4623-4629.
- 99. Lesarri, A.; Cocinero, E. J.; López, J. C.; Alonso, J. L., The Shape of Neutral Valine. *Angew. Chem. Int. Ed.* **2004**, *43*, 605-610.
- 100. Dokmaisrijan, S.; Lee, V. S.; Nimmanpipug, P., The gas phase conformers and vibrational spectra of valine, leucine and isoleucine: An ab initio study. *J. Mol. Struc-THEOCHEM* **2010**, *953*, 28-38.
- 101. Stepanian, S. G.; Reva, I. D.; Radchenko, E. D.; Adamowicz, L., Combined Matrix-Isolation Infrared and Theoretical DFT and ab Initio Study of the Nonionized Valine Conformers. *J. Phys. Chem. A.* **1999**, *103*, 4404-4412.
- 102. Cocinero, E. J.; Lesarri, A.; Grabow, J.-U.; López, J. C.; Alonso, J. L., The Shape of Leucine in the Gas Phase. *ChemPhysChem* **2007**, *8*, 599-604.
- 103. Stepanian, S. G.; Ivanov, A. Y.; Adamowicz, L., Conformational composition of neutral leucine. Matrix isolation infrared and ab initio study. *Chem. Phys.* **2013**, *423*, 20-29.
- 104. Boeckx, B.; Nelissen, W.; Maes, G., Potential Energy Surface and Matrix Isolation FT-IR Study of Isoleucine. *J. Phys. Chem. A.* **2012**, *116*, 3247-3258.
- 105. Hoyau, S.; Ohanessian, G., Interaction of Alkali Metal Cations (Li⁺–Cs⁺) with Glycine in the Gas Phase: A Theoretical Study. *Chem. Eur. J.* **1998**, *4*, 1561-1569.

- 106. Talley, J. M.; Cerda, B. A.; Ohanessian, G.; Wesdemiotis, C., Alkali Metal Ion Binding to Amino Acids Versus Their Methyl Esters: Affinity Trends and Structural Changes in the Gas Phase. *Chem. Eur. J.* **2002**, *8*, 1377-1388.
- 107. Rodgers, M. T.; Armentrout, P. B., Absolute Binding Energies of Lithium Ions to Short Chain Alcohols, $C_nH_{2n+2}O$, n = 1-4, Determined by Threshold Collision-Induced Dissociation. *J. Phys. Chem. A.* **1997**, *101*, 2614-2625.
- 108. Rodgers, M. T.; Armentrout, P. B., Absolute Binding Energies of Sodium Ions to Short Chain Alcohols, $C_nH_{2n+2}O$, n = 1-4, Determined by Threshold Collision-Induced Dissociation Experiments and Ab Initio Theory. *J. Phys. Chem. A.* **1999**, *103*, 4955-4963.
- 109. Klassen, J. S.; Anderson, S. G.; Blades, A. T.; Kebarle, P., Reaction Enthalpies for $M^+L = M^+ + L$, Where $M^+ = Na^+$ and K^+ and L = Acetamide, N-Methylacetamide, N,N-Dimethylacetamide, Glycine, and Glycylglycine, from Determinations of the Collision-Induced Dissociation Thresholds. *J. Phys. Chem.* **1996**, *100*, 14218-14227.
- 110. Rožman, M., Theoretical study of the gas-phase structures of sodiated and cesiated leucine and isoleucine: zwitterionic structure disfavored in kinetic method experiments. *J. Mass Spectrom.* **2005,** *40*, 1357-1361.
- 111. McMeekin, T. L.; Wilensky, M.; Groves, M. L., Refractive indices of proteins in relation to amino acid composition and specific volume. *Biochem. Biophys. Res. Commun.* **1962,** *7*, 151-156.
- 112. Rodgers, M. T.; Armentrout, P. B., Cationic Noncovalent Interactions: Energetics and Periodic Trends. *Chem. Rev.* **2016**, *116*, 5642-5687.
- 113. Rodgers, M. T.; Armentrout, P. B., Discriminating Properties of Alkali Metal Ions Towards the Constituents of Proteins and Nucleic Acids. Conclusions from Gas-Phase and Theoretical Studies. In *The Alkali Metal Ions: Their Role for Life*, Sigel, A.; Sigel, H.; Sigel, R. K. O., Eds. Springer International Publishing: Cham, 2016; pp 103-131.
- 114. Zhao, Y.; Truhlar, D. G., The M06 suite of density functionals for main group thermochemistry, thermochemical kinetics, noncovalent interactions, excited states, and transition

elements: two new functionals and systematic testing of four M06-class functionals and 12 other functionals. *Theor. Chem. Acc.* **2008**, *120*, 215-241.

Table 1. Relative enthalpies at 0 K (Gibbs energies at 298 K) in kJ mol^{-1} of distinctive low-lying K^+Gly and K^+Ala complexes^a

Amino Acid	Conformation	Theory			
		B3LYP ^b	B3P86 ^b	MP2 ^b	B3LYP-
					GD3BJ ^c
Glycine	[CO]cc	0.0 (0.0)	0.0 (0.0)	2.6 (2.2)	0.57 (0.0)
	TS[CO/CO,OH]cc	0.5 (5.3)	0.2 (5.0)	1.0 (5.4)	0.64 (4.9)
	[CO,OH]cc	0.6 (1.0)	0.3 (0.7)	0.0 (0.0)	0.0 (0.9)
	[N,CO]tt	3.9 (6.8)	6.4 (9.4)	2.8 (5.3)	0.6 (3.4)
	TS[CO,OH/CO ₂ ⁻]	11.0 (15.4)	5.2 (9.6)	8.5 (12.5)	10.1 (13.3)
	$[\mathrm{CO_2}^-]\mathrm{cc}$	12.1 (15.6)	10.9 (14.4)	9.6 (12.9)	11.6 (14.7)
	[N,OH]tc	41.9 (44.3)	45.8 (48.2)	35.7 (37.7)	36.4 (38.6)
	[N]tt	50.9 (48.8)	52.8 (51.0)	47.5 (45.4)	48.5 (46.3)
	[OH]tt	83.5 (81.6)	88.6 (86.7)	79.8 (77.4)	81.3 (79.3)
Alanine	[CO,OH]cc	0.0 (0.8)	0.0 (0.5)	0.0 (0.0)	0.0 (0.7)
	TS[CO,OH/CO]cc	0.7 (4.7)	0.8 (4.5)	2.9 (6.1)	1.1 (4.6)
	[CO]cc	1.2 (0.0)	1.5 (0.0)	4.5 (2.5)	1.7 (0.0)
	[N,CO]tts	4.3 (7.3)	7.4 (10.1)	2.0 (4.2)	1.2 (4.1)
	TS[CO,OH/CO ₂ ⁻]cc	5.9 (9.9)	0.8 (4.5)	5.5 (8.7)	5.3 (9.1)
	$[\mathrm{CO_2}^-]\mathrm{cc}$	5.6 (8.6)	5.1 (7.7)	5.6 (7.7)	5.3 (7.9)
	$[N,CO]tt_A$	6.1 (8.8)	9.0 (11.4)	5.2 (7.1)	2.7 (5.2)
	[N,OH]tc _A	39.5 (41.8)	43.6 (45.7)	33.21 (34.72)	33.6 (35.8)
	[N,OH]tcs	40.4 (42.7)	45.0 (47.1)	33.16 (34.66)	33.2 (35.5)
	[N]tt	51.3 (49.7)	54.0 (52.2)	47.2 (44.9)	46.1 (43.2)
	[OH]tt	86.3 (83.7)	92.1 (89.3)	81.0 (77.6)	81.5 (80.6)

^aGibbs energies are in parentheses. Energies include ZPE corrections with frequencies scaled by

0.989. Lowest energy for an isomer at each level of theory is bolded. bAll calculations were performed at the stated level of theory with the 6-311+G(2d,2p) basis set with geometries calculated at the B3LYP/6-311+G(d,p) level of theory. cAll calculations were performed at the B3LYP-GD3BJ/6-311+G(2d,2p)//B3LYP-GD3BJ/6-311+G(d,p) level of theory.

Table 2. Relative enthalpies at 0 K (Gibbs energies at 298 K) in kJ mol^{-1} of distinctive low-lying K^+hAla and K^+Val complexes^a

Amino Acid	Conformation	Theory				
		B3LYP ^b	B3P86 ^b	MP2 ^b	B3LYP- GD3BJ ^c	
Homoalanine	[CO,OH]cc(t)	0.0 (0.6)	0.0 (0.4)	0.0 (0.0)	1.2 (0.4)	
	TS[CO,OH/CO]cc(t)	1.1 (4.9)	1.2 (4.8)	3.6 (6.8)	2.8 (4.8)	
	[CO]cc(t)	1.8 (0.0)	2.0 (0.0)	5.2 (2.9)	3.4 (0.0)	
	$[N,CO]tt_S(g)$	7.7 (10.3)	7.1 (9.4)	18.0 (20.0)	0.0 (2.0)	
	$[N,CO]tt_S(t)$	5.3 (7.4)	8.4 (10.3)	2.8 (4.4)	1.6 (2.4)	
	TS[CO,OH/CO ₂ ⁻]cc(t)	4.9 (8.3)	0.1 (3.2)	4.8 (7.5)	5.6 (7.5)	
	$[\mathrm{CO_2}^-]\mathrm{cc}(t)$	4.3 (6.5)	3.9 (5.9)	4.5 (6.2)	5.0 (5.7)	
	$[N,OH]tc_A(t)$	40.7 (42.0)	44.6 (45.6)	34.6 (35.3)	35.7 (35.6)	
	[N]tc(t)	62.1 (59.9)	65.2 (62.7)	56.5 (53.6)	55.7 (52.3)	
	[N]tc(g_)	64.5 (60.7)	67.4 (63.3)	57.5 (53.0)	57.2 (52.5)	
Valine	$[CO,OH]cc(g_+)$	0.0 (0.1)	0.0 (0.0)	0.0 (0.0)	$1.4(0.0_1)$	
	TS[CO,OH/CO]cc(g ₊)	1.5 (4.7)	1.6 (4.8)	4.2 (7.3)	3.3 (4.6)	
	$[CO]cc(g_+)$	2.2 (0.0)	2.5 (0.1)	5.7 (3.3)	4.0 (0.0)	
	$TS[CO,OH/CO_2^-]cc(g_+)$	4.1 (6.6)	-0.7 (1.6)	4.0 (4.3)	4.8 (5.6)	
	$[\mathrm{CO_2}^-]\mathrm{cc}(\mathrm{g}_+)$	2.4 (4.0)	2.1 (3.6)	2.6 (4.2)	3.1 (3.0)	
	$[N,CO]tt_S(g_+)$	6.2 (7.8)	9.1 (10.6)	2.5 (4.0)	0.0 (0.9)	
	$[N,CO]tt_A(g_+)$	6.3 (7.9)	8.9 (10.4)	4.9 (6.3)	3.7 (3.7)	
	$[N,OH]tc_A(g_+)$	40.2 (40.9)	43.8 (44.4)	24.1 (24.7)	35.5 (34.6)	
	$[N]tt(g_+)$	51.6 (50.5)	54.0 (52.8)	45.7 (44.5)	44.9 (43.1)	

^aGibbs energies are in parentheses. Energies include SPE corrections with frequencies scaled by 0.989. Lowest energy for an isomer at each level of theory is bolded. ^bAll calculations are

performed at the stated level of theory with the 6-311+G(2d,2p) basis set with geometries calculated at the B3LYP/6-311+G(d,p) level of theory. ^cAll calculations are performed at the B3LYP-GD3BJ/6-311+G(2d,2p)//B3LYP-GD3BJ/6-311+G(d,p) level of theory.

Table 3. Relative enthalpies at 0 K (Gibbs energies at 298 K) in kJ mol^{-1} of distinctive low-lying K⁺Leu and K⁺Ile complexes^a

Amino	Conformation	Theory			
Acid					
		B3LYP ^b	B3P86 ^b	MP2 ^b	B3LYP-
					GD3BJ ^c
Leucine	[CO,OH]cc(tg ₊)	0.0 (0.3)	0.0 (0.0 ₃)	0.0 (0.0)	0.2 (0.04)
	TS[CO,OH/CO]cc(tg+)	1.5 (5.0)	1.6 (4.9)	4.1 (7.4)	2.1 (5.1)
	$[CO]cc(tg_+)$	2.1 (0.0)	2.4 (0.0)	5.6 (3.2)	2.7 (0.0)
	TS[CO,OH/CO ₂ ⁻]cc(tg ₊)	4.5 (7.8)	-0.3 (2.4)	4.5 (7.2)	4.4 (6.9)
	$[\mathrm{CO_2}^-]\mathrm{cc}(\mathrm{tg}_+)$	3.5 (5.3)	3.2 (4.8)	3.9 (5.4)	3.3 (4.6)
	$[N,CO]tt_S(tg_+)$	5.1 (7.1)	8.2 (10.0)	2.1 (3.9)	0.0 (2.2)
	$[N,OH]tc_S(tg_+)$	41.0 (42.4)	45.5 (46.7)	32.8 (33.9)	32.2 (33.9)
	[N]tt(g_c)	62.4 (62.2)	65.8 (65.3)	54.7 (54.2)	53.9 (54.6)
Isoleucine	[CO,OH]cc(g-t)	0.0 (0.5)	0.0 (0.3)	0.0 (0.0)	$2.0(0.0_1)$
	TS[CO,OH/CO]cc(g-t)	1.8 (5.3)	1.9 (5.2)	4.7 (7.7)	4.1 (4.8)
	[CO]cc(g-t)	2.3 (0.0)	2.6 (0.0)	5.8 (2.9)	4.8 (0.0)
	TS[CO,OH/CO ₂ ⁻]cc(g-t)	3.8 (6.4)	-1.1 (1.3)	3.7 (5.8)	5.2 (5.3)
	$[\mathrm{CO_2}^-]\mathrm{cc}(\mathrm{g-t})$	1.8 (3.6)	1.5 (3.1)	2.1 (3.4)	3.2 (2.4)
	$[N,CO]tt_S(g-t)$	6.1 (8.1)	8.9 (10.7)	2.0 (3.4)	0.0 (0.7)
	$[N,CO]tt_A(g-t)$	6.1 (8.0)	8.7 (10.4)	4.5 (5.8)	4.2 (3.6)
	$[N,OH]tc_S(g-t)$	40.2 (42.8)	44.2 (46.6)	31.0 (33.1)	30.7 (31.8)
	[N]tt(tt)	59.5 (59.4)	62.5 (62.2)	52.7 (52.1)	53.4 (51.5)

^aGibbs energies are in parentheses. Energies include SPE corrections with frequencies scaled by 0.989. Lowest energy for an isomer at each level of theory is bolded. ^bAll calculations are performed at the stated level of theory with the 6-311+G(2d,2p) basis set with geometries

calculated at the B3LYP/6-311+G(d,p) level of theory. $^{\rm c}$ All calculations are performed at the B3LYP-GD3BJ/6-311+G(2d,2p)//B3LYP-GD3BJ/6-311+G(d,p) level of theory.

 $Table \ 4. \ Fitting \ Parameters \ of \ Equation \ 1, \ Threshold \ Energies \ at \ 0 \ K, \ and \ Entropies \ of \ Activation \ at \ 1000 \ K \ for \ Cross \ Sections \ of \ the \ TCID \ Reactions \ of \ K^+AA^a$

AA	Ionic Reactant	Neutral Product	σ_0	n	E_0 (eV)	$\Delta S_{1000}^{\ddagger} \left(\mathrm{J/(K\ mol)} \right)$
Gly	[CO,OH]cc	ttt	23.0 (1.6)	1.0 (0.1)	1.23 (0.04)	21.4 (0.1)
	[CO]cc	ttt	23.1 (2.0)	1.0 (0.1)	1.22 (0.05)	17.2 (2.2)
Ala	[CO,OH]cc	ttt	25.4 (1.6)	1.0 (0.1)	1.26 (0.04)	29.9 (0.1)
	[CO]cc	ttt	25.0 (0.9)	1.0 (0.1)	1.24 (0.04)	21.3 (0.1)
hAla	[CO,OH]cc(t)	ttt(t)	36.0 (7.0)	1.0 (0.1)	1.31 (0.05)	32.7 (0.1)
	[CO]cc(t)	ttt(t)	34.3 (6.1)	1.0 (0.1)	1.28 (0.05)	24.0 (0.1)
Val	$[CO,OH]cc(g_+)$	ttt(c)	35.8 (1.2)	1.0 (0.1)	1.30 (0.04)	34.9 (1.4)
	$[\mathrm{CO}]\mathrm{cc}(\mathrm{g}_{^{+}})$	ttt(c)	35.5 (0.9)	1.0 (0.1)	1.28 (0.05)	26.4 (2.2)
Leu	$[CO,OH]cc(tg_+)$	$ttt(tg_+)$	36.0 (0.9)	1.0 (0.1)	1.32 (0.05)	35.3 (2.5)
	$[CO]cc(tg_+)$	$ttt(tg_+)$	37.6 (2.4)	0.9 (0.2)	1.32 (0.07)	26.7 (3.5)
Ile	[CO,OH]cc(g-t)	ttt(g_t)	35.4 (1.6)	1.0 (0.2)	1.33 (0.05)	38.8 (0.1)
	[CO]cc(g-t)	ttt(g_t)	35.5 (1.8)	1.0 (0.2)	1.30 (0.05)	29.5 (0.1)

^aUncertainties in parentheses.

Table 5. Enthalpies and Free Energies of Reaction at 0 and 298 K for K⁺-AA Bond Dissociation ^a

Reaction	Reactant	$\Delta { m H_0}^b$	ΔH_{298} - $\Delta H_0^{\ c}$	ΔH_{298}	$\mathrm{T}\Delta\mathrm{S}_{298}^{\;\;c}$	ΔG_{298}
$K^+(Gly) \to K^+ + Gly$	[CO,OH]	118.8 (3.7)	0.8 (0.1)	119.6 (3.7)	28.2 (0.7)	97.4 (3.8)
	[CO]	117.8 (4.6)	0.8 (0.1)	118.6 (4.6)	27.7 (0.7)	90.9 (4.6)
$K^+(Ala) \rightarrow K^+ + Ala$	[CO,OH]	121.3 (3.4)	1.4 (0.1)	122.7 (3.4)	29.5 (0.6)	93.0 (3.5)
	[CO]	119.9 (4.3)	1.4 (0.1)	121.3 (4.3)	29.3 (0.6)	92.0 (4.4)
$K^+(hAla) \rightarrow K^+ + hAla$	[CO,OH]	126.8 (4.6)	1.5 (0.1)	128.3 (4.6)	30.4 (0.6)	97.9 (4.7)
	[CO]	123.7 (5.2)	1.5 (0.1)	125.2 (5.2)	30.4 (0.6)	94.8 (5.3)
$K^+(Val) \rightarrow K^+ + Val$	[CO,OH]	125.9 (4.1)	1.5 (0.1)	127.4 (4.1)	30.6 (0.6)	96.8 (4.2)
	[CO]	123.1 (4.7)	1.3 (0.1)	124.4 (4.7)	28.1 (0.6)	96.3 (4.8)
$K^+(Leu) \rightarrow K^+ + Leu$	[CO,OH]	127.6 (5.0)	1.5 (0.1)	129.1 (5.0)	31.2 (0.6)	97.9 (5.1)
	[CO]	127.2 (6.5)	1.3 (0.1)	128.5 (6.5)	28.6 (0.6)	99.9 (6.6)
$K^+(Ile) \rightarrow K^+ + Ile$	[CO,OH]	128.0 (5.1)	1.6 (0.1)	129.6 (5.1)	31.8 (0.6)	97.8 (5.2)
	[CO]	125.3 (5.3)	1.3 (0.1)	126.6 (5.3)	29.0 (0.6)	97.6 (5.4)

^a Uncertainties in parentheses.

^b Experimental values from Table 4.

^c Calculated using standard formulas and molecular constants calculated at the B3LYP/6-311+G(d,p) level.

Table 6. Experimental and Theoretical K+-AA Bond Dissociation Energies at 0 K (kJ/mol)

		Experiment		Theory ^a			
AA	Ionic Reactant	TCID ^b	KM ^c	B3LYP ^d	B3P86 ^d	MP2 ^d	B3LYP-GD3BJ ^e
Gly	cc	118.3 (4.2)	119 (11)	116.6 / 116.0	119.9 / 119.2	116.4 / 112.7	124.1 / 123.2
Ala	cc	120.6 (3.9)	123 (11)	121.3 / 120.6	125.0 / 124.4	120.2 / 116.3	128.9 / 128.3
hAla	cc(t)	125.2 (4.9)		123.6 / 123.4	127.4 / 126.7	122.6 / 118.3	131.7 / 130.9
Val	$cc(g_+)$	124.5 (4.4)	127 (11)	125.0 / 124.3	128.6 / 128.0	123.8 / 119.7	133.7 / 132.9
Leu	$cc(tg_+)$	127.4 (5.8)	128 (11)	125.8 / 125.0	129.6 / 128.9	124.6 / 120.7	133.8 / 133.0
Ile	cc(gt)	126.7 (5.2)	129 (11)	126.6 / 125.9	130.2 /129.5	125.8 / 121.6	135.3 / 134.5
	$\mathrm{MAD^f}$		2 (1)	1.0 (0.7) / 1.3 (1.1)	3.0 (1.2) / 2.3 (1.2)	1.5 (1.0) / 5.6 (1.1)	7.5 (1.4) / 6.7 (1.5)

^a Values in italics include BSSE corrections. ^b TCID experimental values from Table 4, average of [CO,OH] and [CO] threshold energies. Uncertainties in parentheses. ^c Kinetic method (KM) results from Tsang et al. ⁵² ^d Calculations performed at the B3LYP, B3P86, or MP2/6-311+G(2d,2p)// B3LYP/6-311+G(d,p) level including ZPE corrections. For B3LYP and B3P86, these refer to the average value for the [CO,OH] and [CO] isomers, whereas for MP2, they are a 2:1 average of these two isomers. ^c Calculations performed at B3LYP-GD3BJ/6-311+G(2d,2p)// B3LYP-GD3BJ/6-311+G(d,p) level including ZPE corrections. Values correspond to average of [CO,OH] and [CO] isomers. ^f Calculated mean absolute deviations (MADs) from TCID experimental values.

Figure Captions

Figure 1. Cross sections extrapolated to zero-pressure conditions for collisions induced dissociation of K^+AA (AA = Gly, Ala, hAla, Val, Leu, and Ile) with Xe as a function of kinetic energy in the center-of-mass frame (lower x-axis) and the laboratory frame (upper x-axis). Solid lines show the best model of the data assuming a [CO,OH] reactant using Eq. 1 with convolution over the neutral and ionic kinetic and internal energy distributions. Dashed lines show the best model of the data excluding the neutral and ion kinetic and internal energy distributions.

Figure 2. Lowest-energy structures of K⁺Ala for each chelation site found, calculated at the B3LYP/6-311+G(d,p) level of theory. Hydrogen bonds are indicated by dotted lines. Potassiumligand noncovalent bonds are indicated by thick dashed lines. Relative energies (kJ/mol) at 298 K from Table 1 are shown for the B3LYP, B3P86, MP2, and B3LYP-GD3BJ levels of theory, respectively. Values at 0 K are listed in Table 1.

Figure 3. Lowest-energy structures of K⁺AA (AA = hAla, Val, Leu, and Ile) calculated at the B3LYP/6-311+G(d,p) level of theory. Hydrogen bonds are indicated by dotted lines. Potassiumligand noncovalent bonds are indicated by thick dashed lines. Relative energies (kJ/mol) at 298 K from Tables 2 and 3 are shown for the B3LYP, B3P86, MP2, and B3LYP-GD3BJ levels of theory, respectively. Values at 0 K can be found in the Tables.

Figure 4. A potential surface calculated at the B3LYP/6-311+G(d,p) level for interconversion between K⁺Ala[CO]cc and K⁺Ala[CO,OH]cc as a function of KOC angle. Relative ZPEs calculated at the B3LYP/6-311+G(2d,2p) level scaled to match the energy of the TS are indicated by horizontal lines.

Figure 5. Bond dissociation energies (kJ/mol) for K⁺AA at 0 K determined by TCID (red triangles, this study), KM (blue circles, Tsang et al.⁵²), and B3LYP theory (inverted open triangles, this study) plotted versus polarizabilities (Å³) of the AA. The dashed line is a linear regression fit of all the TCID data, whereas the solid line excludes hAla.

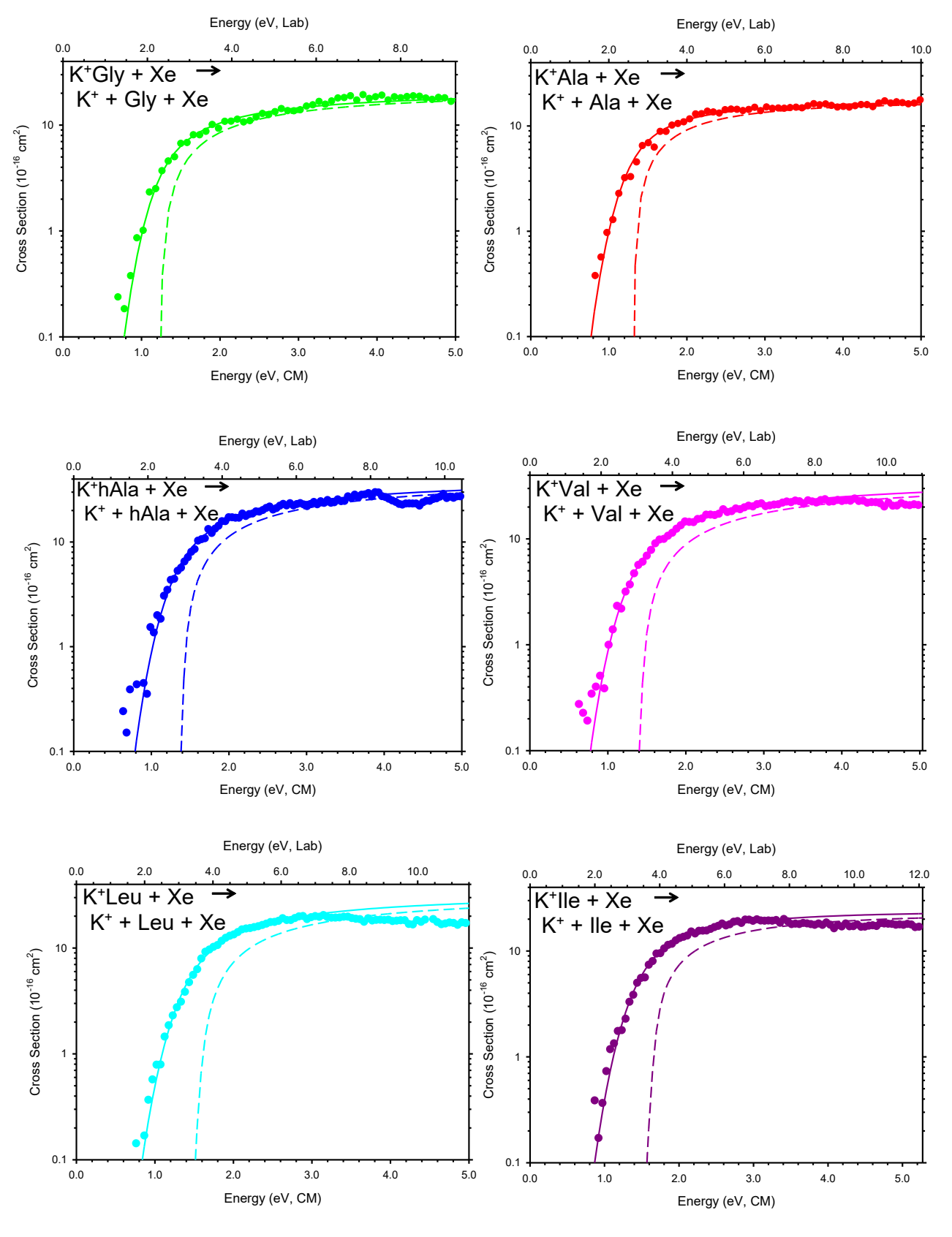


Figure 1

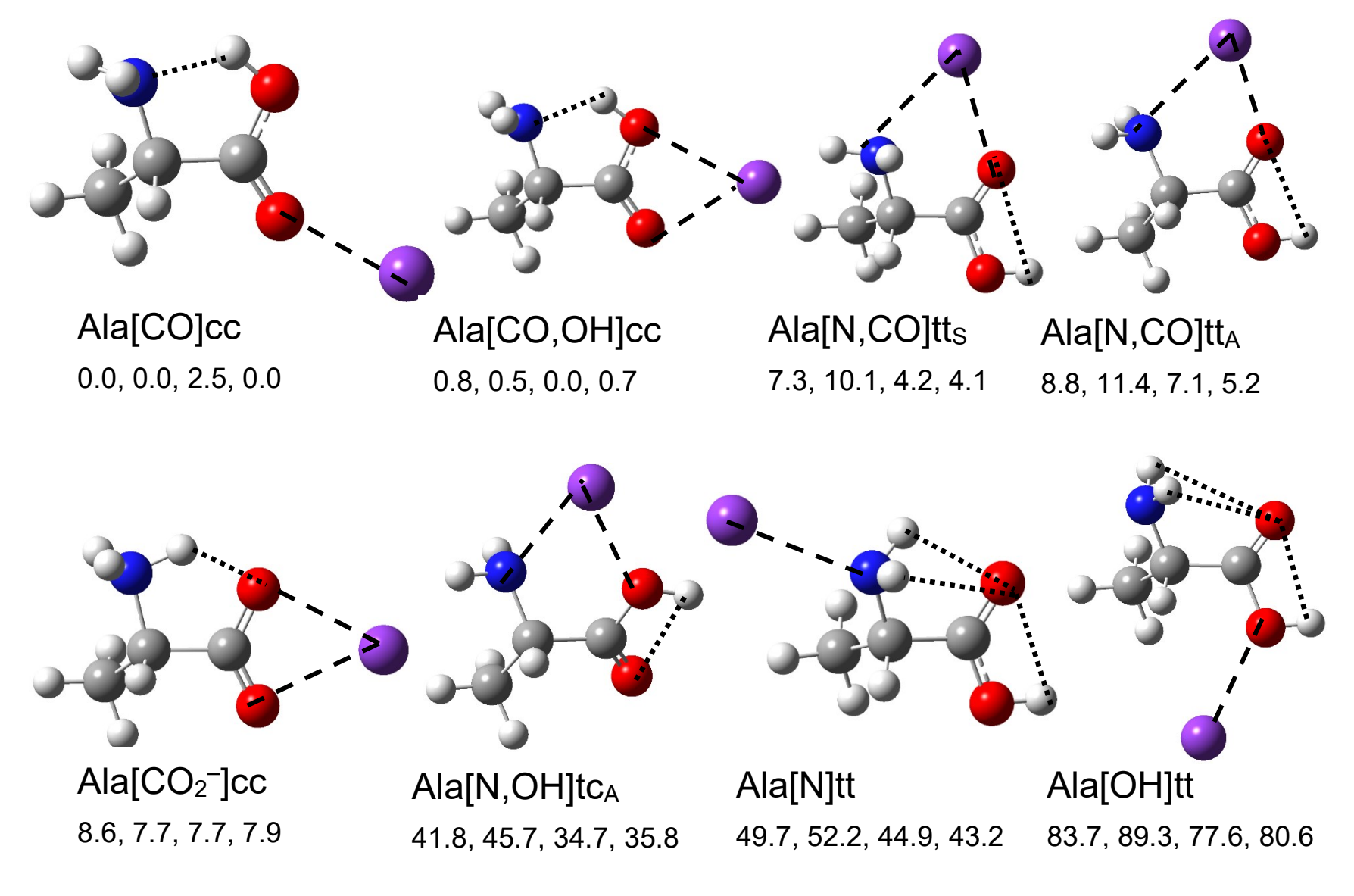


Figure 2

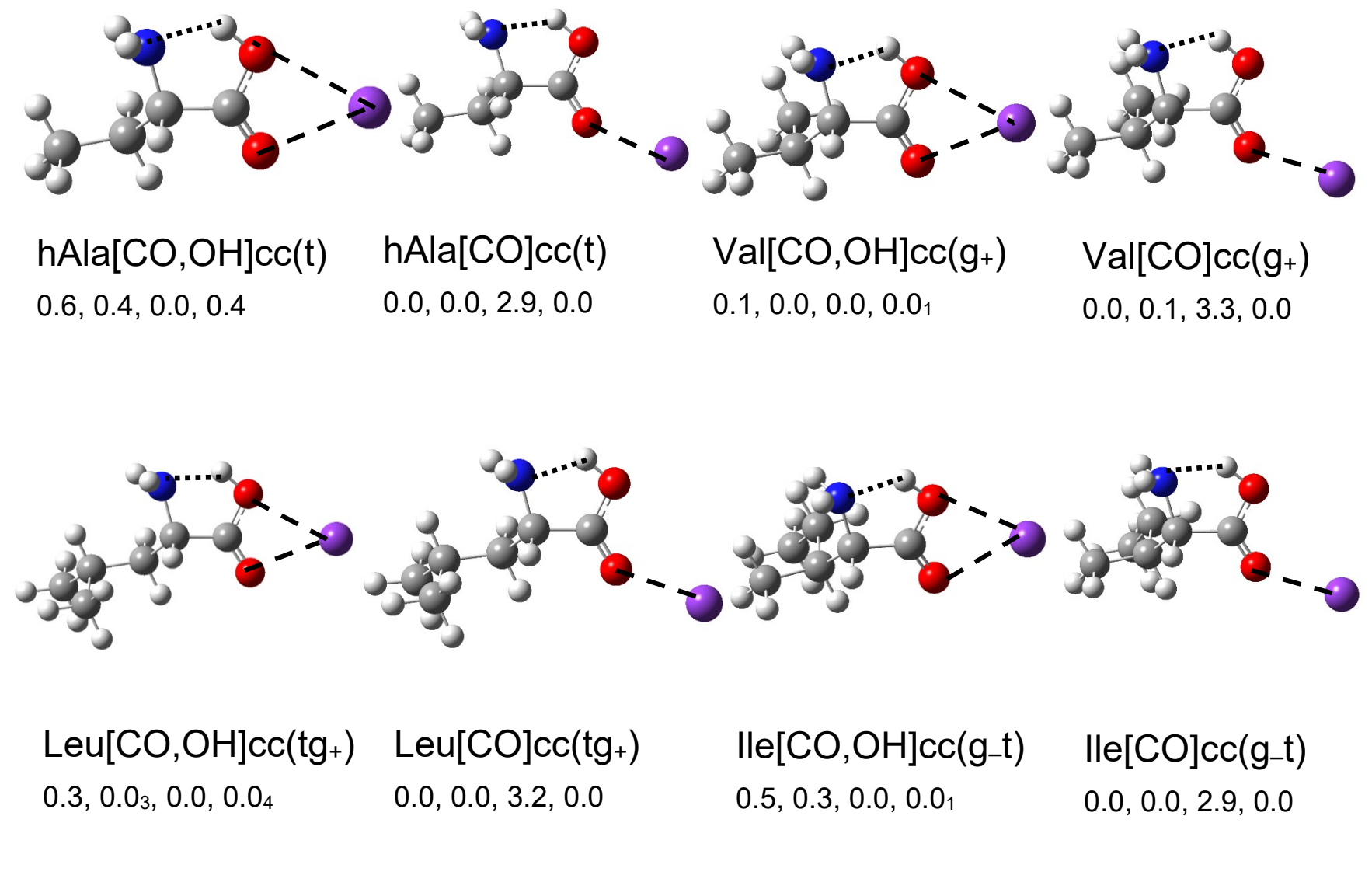


Figure 3

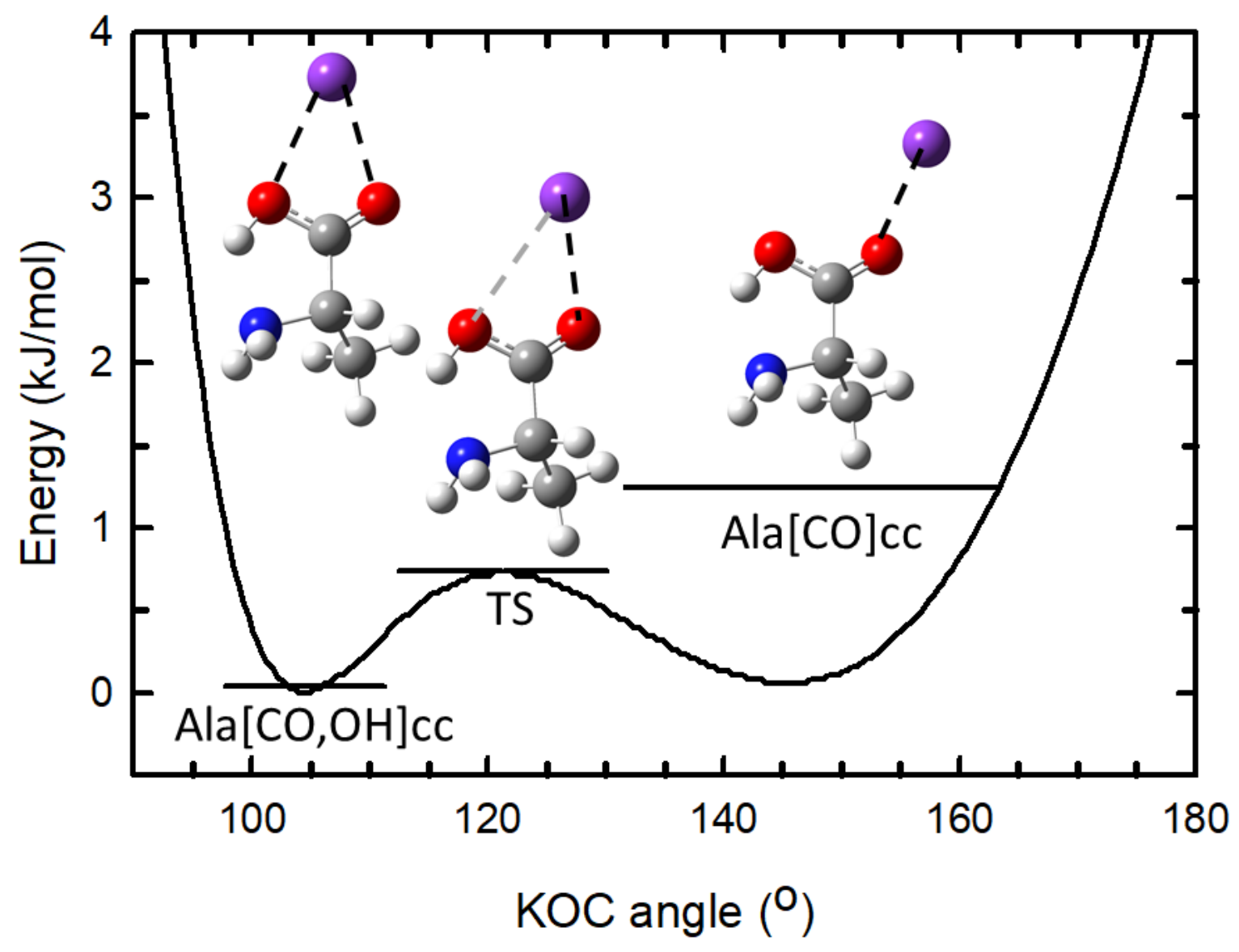


Figure 4

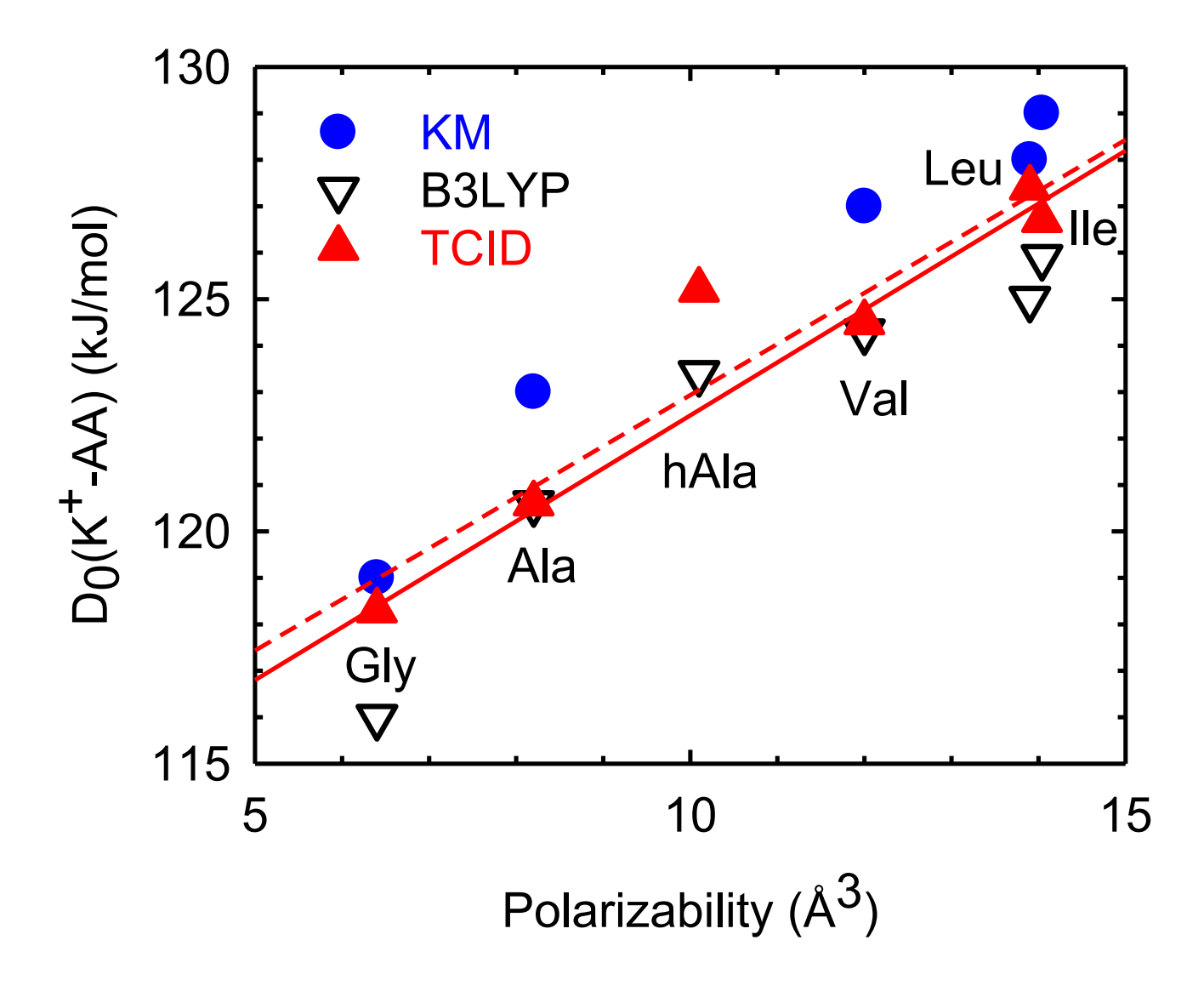
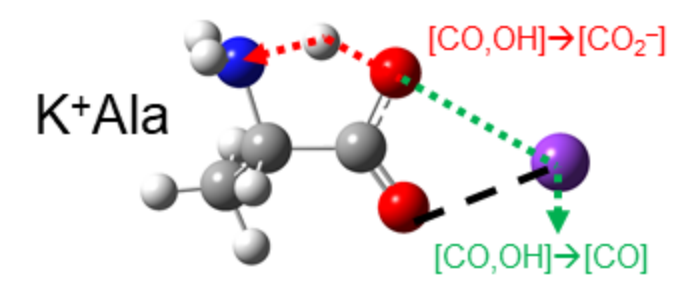


Figure 5

For Table of Contents Use Only

Potassium Binding Interactions with Aliphatic Amino Acids: Thermodynamic and Entropic Effects Analyzed via a Guided Ion Beam and Computational Study

Roland M. Jones III, Taylor Nilsson, Samantha Walker, and P. B. Armentrout*



Binding energies of potassiated aliphatic amino acids are experimentally determined and double well potentials connecting three low energy conformers of these complexes are explored computationally.